LBL-1807

c.1

MEASUREMENT OF INTENSITIES OF LOW ENERGY ELECTRON DIFFRACTION BEAMS FROM PLATINUM SURFACES AND FROM ADSORBED OVERLAYERS

John Joseph Wasilczyk
(M.S. thesis)

June 1973

Prepared for the U.S. Atomic Energy Commission
under Contract W-7405-ENG-48

For Reference

Not to be taken from this room

LAWRENCE BERKELEY LABORATORY • UNIVERSITY OF CALIFORNIA • BERKELEY

LBL-1807

c.1

DISCLAIMER

This document was prepared as an account of work sponsored by the United States Government. While this document is believed to contain correct information, neither the United States Government nor any agency thereof, nor the Regents of the University of California, nor any of their employees, makes any warranty, express or implied, or assumes any legal responsibility for the accuracy, completeness, or usefulness of any information, apparatus, product, or process disclosed, or represents that its use would not infringe privately owned rights. Reference herein to any specific commercial product, process, or service by its trade name, trademark, manufacturer, or otherwise, does not necessarily constitute or imply its endorsement, recommendation, or favoring by the United States Government or any agency thereof, or the Regents of the University of California. The views and opinions of authors expressed herein do not necessarily state or reflect those of the United States Government or any agency thereof or the Regents of the University of California.

0 0 0 0 3 9 0 0 0 9 2

TABLE OF CONTENTS

ABSTRACT v

I. Introduction 1

II. Theory 3

A. Basis of Low Energy Electron Diffraction 3

B. Dynamical Scattering Theory as Applied To Low Energy Electron Diffraction 8

C. Surface Structure Nomenclature 30

III. Experimental 35

A. Apparatus 35

B. Samples and Sample Treatment 38

C. General Experimental Procedure 41

D. Intensity Measurement Techniques 42

1. Preliminary Considerations 42

2. Spot Photometer 45

3. Photographic Method 46

E. Intensity Data 61

1. Clean Metal Surfaces 61

2. Adsorbed Overlayer 70

IV. Discussion 80

V. Conclusion 92

Acknowledgements 93

References 95

0 0 0 0 3 9 0 0 0 9 3

MEASUREMENT OF INTENSITIES OF LOW ENERGY ELECTRON DIFFRACTION BEAMS FROM PLATINUM SURFACES AND FROM ADSORBED OVERLAYERS

John Joseph Wasilczyk

Inorganic Materials Research Division, Lawrence Berkeley Laboratory and Department of Chemistry; University of California, Berkeley, California

ABSTRACT

A method for obtaining normalized relative intensities from photographs of the diffraction pattern on the screen of a Varian LEED display apparatus has been developed. The optical density of the diffraction spot on the photograph is measured by a scanning microdensitometer and integrated over the area of the spot. Intensities are calculated from an experimentally determined characteristic curve for the film and then normalized by the incident beam current. Intensities of the diffraction beams from the (111) and (100) faces of platinum and from the surface structure formed by the adsorption of propene on Pt(111) have been measured using this technique. The results from Pt(111) are compared with intensities calculated by programs based on LEED dynamical scattering theory and show little agreement. Some of the intensity versus voltage curves for the Pt(100) surface are compared with data which were obtained by the spot photometer technique by another investigator[29] and for the most part the agreement is acceptable.

I. INTRODUCTION

The diffraction of low energy electrons was first observed by Davisson and Germer in 1927 in an experiment designed to test the wave hypothesis of DeBroglie.[1] Since then it has developed into an extremely useful technique in modern surface science. Because of the large scattering cross sections of electrons with energies of less than 100 volts, a substantial fraction of the intensity of an incident beam is backscattered and these scattered electrons contain information about the first few layers of the surface. The study of the surface structures of single crystals has shown that in both surface adsorption and deposition ordered structures often form. From the diffraction pattern, the size and shape of the surface unit cell can be determined, but the orientation of the basis of surface atoms to these lattice points and the perpendicular distance of the absorbed layer from the substrate layer can be varied to give a number of models which all result in the same diffraction pattern. To distinguish between these models one must use a scattering theory to calculate intensities and then match them with experimentally measured ones.

Kinematic or single scattering theory which is used in X-ray diffraction work is inadequate since the large scattering cross-sections of the electrons make multiple scattering very probable. A great number of people have worked on developing theoretical approaches to the multiple scattering problem[2] and their formulations have become very sophisticated as they were forced to consider the physics

of most of the processes that occur in the crystal in order to reproduce the experiment. Recently, several notable successes have been achieved in correlating theoretical calculations with experimental data. Duke, Tucker and Larramore,[3] Marcus, Jepsen and Jona,[4] Tong and Rhodin,[5] and Martin and Somorjai[6] have all demonstrated that their procedures reproduce the experimental results for the low index faces of face-centered cubic aluminum. Pendry, working primarily on nickel, has also had substantial success.[7] With the hope that the theory is now capable of handling more complicated atoms with stronger scattering power, the intensities of diffraction beams from the Pt(111) surface, the Pt(100) surface, and from an absorbed layer of propene on the (111) surface of platinum were measured by means of a photographic technique. The diffraction pattern was photographed and the optical densities of diffraction spots on the film negative were measured by a scanning microdensitometer. Intensities were calculated from an experimentally determined characteristic curve for the film and then normalized by the incident beam current. The results from Pt(111) were compared with intensities calculated by computer programs using dynamical scattering theory. The intensities from the Pt(100) surface were compared with data obtained with a spot photometer by another investigator.

0 0 0 0 5 9 0 0 8 9 5

II. THEORY

A. Basis of Low Energy Electron Diffraction

In 1924 DeBroglie made a major contribution towards the advancement of our understanding of matter. It had already been shown that light had to be treated by both a corpuscular and a wave theory if its behavior was to be successfully explained. DeBroglie advanced the hypothesis that all matter can be treated as both a particle and a wave. He suggested that the two treatments were related by the equation

$$\lambda = \frac{h}{p} = \frac{h}{mV} = \frac{h}{(2mE)^{1/2}} \tag{1}$$

which connects the wavelength of matter considered as a wave with momentum when matter is thought of as a particle. If all matter had wavelike properties, diffraction of particles should be observed provided that the momentum was chosen to give the proper wavelength. The Davisson-Germer experiment showed that when the wavelength of an incident electron beam was equal to or less than the interatomic distance of the target crystal, the electrons were diffracted by the rows of surface atoms like light is diffracted by a two-dimensional line grating. By substituting values for an electron into Eq. (1) we get

$$\lambda(\text{Å}) = \sqrt{\frac{150.4}{V}} \tag{2}$$

where V is the potential difference in volts between the electron and the target. Incoming electrons are scattered primarily by a coulombic interaction with the crystal's potential. The large collision cross sections for these interactions mean that most of the back-scattered electrons are reflected from the surface or vicinity and because of this the electrons do not detect the three dimensional periodicity of the crystal potential. In effect, the perfect periodic potential in the two dimensions parallel to the surface results in a two dimensional diffraction pattern since the scattered electrons destructively interfere except along beams in space with well-defined direction.

If the incident electron beam is considered from the wave viewpoint it can be described by[8]

$$A(r) = A(o)\ \exp(i(\vec{k}\cdot\vec{r} - \omega t)) \tag{3}$$

where A(r) is the amplitude at some point r, A(o) the amplitude at an arbitrary origin, $\vec{k}$ the wavevector and ω the angular frequency. $\vec{k}$ can be related to wavelength and therefore to momentum since $|k| = 2\pi/\lambda$. The condition of elastic scattering requires that

$$|k'|^2 = |k^\circ|^2 \tag{4}$$

where $\vec{k}'$ = wavevector of the scattered beam and $\vec{k}^\circ$ = wavevector of the incident beam since

$$|k| = \frac{2\pi}{\lambda} = \frac{2\pi(2mE)^{1/2}}{h} \tag{5}$$

and $|k|^2$ is directly proportional to energy. Diffraction by a two dimensional periodic potential at the surface requires that

$$\vec{k}'_{\parallel} = \vec{k}^{0}_{\parallel} + \vec{G}_{\parallel} \tag{6}$$

where $\vec{k}_{\parallel}$ is the parallel component of the wavevector and $\vec{G}_{\parallel}$ is a parallel reciprocal lattice vector defined by the surface lattice.

$$\vec{G}_{\parallel} = 2\pi \left(\frac{h(\vec{b}\times\hat{z})}{\vec{a}\cdot\vec{b}\times\hat{z}} + \frac{k(\hat{z}\times\vec{a})}{\vec{a}\cdot\vec{b}\times\hat{z}} \right) \tag{7}$$

where $\vec{a}$ and $\vec{b}$ are the basis vectors of the surface lattice expressed in terms of unit vectors $\hat{x}$ and $\hat{y}$, $\hat{z}$ is a unit vector in the perpendicular direction and h and k are integers. Because energy is conserved (Eq. 4) the perpendicular component of $\vec{k}'$ is determined by Eq. (6).

$$|k^{\circ}|^2 = |k'|^2 = |k'_{\parallel}|^2 + |k'_{\perp}|^2 \tag{8}$$

$$|k'_{\perp}|^2 = |k^{\circ}|^2 - |k^{\circ}_{\parallel}|^2 - |G_{\parallel}|^2 \tag{9}$$

$$|k'_{\perp}| = \sqrt{|k^{\circ}|^2 - |k^{\circ}_{\parallel}|^2 - |G_{\parallel}|^2} \tag{10}$$

Thus for a given reciprocal lattice vector, k' is determined by the energy and the direction of the incident beam.

However, this determination of the wavevector of the scattered beam assumes that there is only one collision, actually, multiple scattering plays an important role in the case of LEED as was already mentioned. Because of the large scattering cross sections, the scattered beam can become diffracted again with the restriction that

$$\vec{k}_{\parallel}'' = \vec{k}_{\parallel}' + \vec{G}_{\parallel} \quad . \tag{11}$$

This condition for double diffraction can be extended to include tertiary and higher order scattering and its effects can be seen in the intensity profiles of the beams.

Earlier it was stated that the diffraction beams resulted from the two-dimensional periodicity of the surface potential and that the diffraction condition was expressed by Eq. (6). The effect of the periodicity of the crystal potential in the z direction is contained in the intensity of the beams and can be expressed by a similiar diffraction condition

$$\vec{k}_{\perp}' = \vec{k}_{\perp}^{\circ} + \vec{G}_{\perp} \quad . \tag{12}$$

If the electrons were all scattered by the first layer of the surface and never detected the vertical periodicity of the potential $k_{\perp}$ could assume any value as determined by Eq. (10). For a given reciprocal lattice vector and keeping the direction of the incident beam constant, one would expect the intensity to be a monotonic function of energy. (Fig. II-1A)

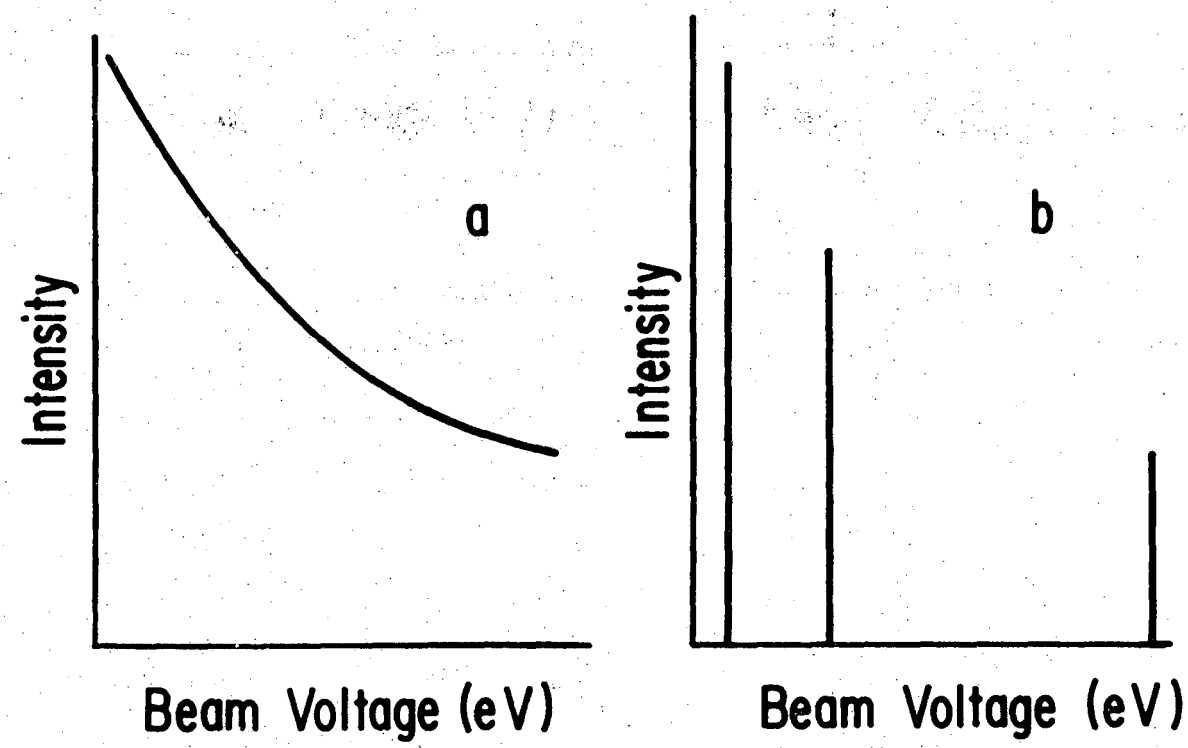

XBL 703-561

Fig. II-1. Intensity versus voltage curves for 2-D and 3-D diffraction.

However, if the electrons penetrated deeply enough to experience the full three-dimensional periodicity of the potential Eqs. (6) and (12) would have to be satisfied simultaneously for single diffraction. This kinematic treatment would give an I. vs V. curve like b in Fig. II-1 where the sharp peaks are the energies at which the Bragg conditions are fulfilled. An intensity versus energy curve for LEED is continuous as in two-dimensional diffraction but shows a number of strong broad peaks indicating that the vertical periodicity of the potential does have some effect. Peaks other than the kinematic ones predicted by Eqs. (6) and (12) indicate that multiple scattering does provide an important contribution to the scattered intensities and that equations similiar to Eq. (11) but for the perpendicular components must also be satisfied. Positions of intensity peaks can then be predicted from knowledge of the surface and experimental geometry by considering all diffraction events but the shape of the intensity peaks depends upon the details of the actual crystal potential and the extent to which different order scattering events contribute to the same peak.

B. Dynamical Scattering Theory As Applied To Low Energy Electron Diffraction

Analysis of the diffraction pattern at a given energy of the surface together with the angle of incidence of the electron beam gives one the direction of both the incident and scattered beams. It has been shown that this can then be used to find the surface reciprocal lattice vectors which determine the size and shape of the

surface unit cell. The type of surface atoms, their orientation to these lattice points, and the perpendicular distance between layers all affect the crystal potential and they can only be determined by measurement of the intensity profiles of the diffracted beams and by consideration of their relationship to the shape, magnitude, and position of the intensity maxima. This is what LEED dynamical scattering theory hopes to do.

The literature is filled with papers in which people tried to use various simplified approaches to the problem during the early days of investigation and came up with results that bore at best only a vague resemblence to experiments. Since detailed reviews of this work are available[2] we will not cover it but will consider some of the various methods which have been developed that show promise of producing theoretical intensities that compare with the experimental ones. Primary attention will be paid to those techniques which displayed the first successful model of one of the phenomena important in determining the electron intensities.

Essentially two approaches to the problem of scattering a low energy electron beam upon a crystal have been developed. Multiple scattering theory was used by Beeby to derive a formalism based upon scattering matrices within a layer of the crystal and then considering scattering between layers. This method, using a Green's function in the integral form of the Schroedinger wave equation assumes symmetry only within the plane of the crystal's layers and so is readily applied to a surface layer that is quite different from the substrate

layer. The programs of Duke, Tucker and Larramore, Tong and Rhodin, and Martin and Somorjai use this type of formalism.

The second method works with the differential form of the wave equation and solves for the wave function within the crystal by assuming it to be a perfect, infinite crystal. The wave equation is then solved outside of the crystal and the two wave functions and their derivatives are matched at the boundary of the crystal surface. This approach, derived by Bondreaux and Heine, is used by Pendry and Marcus and Jepsen.

Beeby's Scattering Matrix Formalism

Beeby's method considers elastic scattering only and computes the scattering amplitude for incident electrons scattered by a muffin-tin type potential. The muffin-tin approximation assumes that the crystal's potential can be considered a series of non-overlapping spherical potentials with V=0 between the spheres.[9] If these ion-core potentials are at site R and designated $V_R(\vec{r})$,

$$V(\vec{r}) = \sum_R V_R(\vec{r}-\vec{R}) .$$

The incoming beam has wavevector $\vec{k}$ and is considered to be a plane wave. So looking at the outgoing wave at a distance large compared to the size of the crystal, the intensity of the wave scattered by V(r) would be

$$I(\vec{k}-\vec{k}') \propto \left| \int \exp(-i\vec{k}'\cdot\vec{r}')T(\vec{r}',\vec{r})\exp(i\vec{k}\cdot\vec{r})d\vec{r}d\vec{r}' \right|^2 \qquad (13)$$

where $T(\vec{r}',\vec{r})$ is defined as the scattering matrix of the whole crystal and can be written as the sum of the scattering matrices of each atom.

$$T(\vec{r}',\vec{r}) = \sum_{R} t_R(\vec{r}'-\vec{R}, \vec{r}-\vec{R}) + \sum_{R\neq R'} t_{R'}(\vec{r}'-\vec{R}', \vec{r}''-\vec{R}') \, G_0(\vec{r}''-\vec{r}''')$$

$$t_R(\vec{r}'''-\vec{R}, \vec{r}-\vec{R}) \, d\vec{r}'' \, d\vec{r}''' + \ldots \qquad (14)$$

where the multiple scattering matrix for each atom t_R would be

$$t_R(\vec{r}',\vec{r}) = V_R(\vec{r}') \, \delta(\vec{r}-\vec{r}') + \int V_R(\vec{r}') \, G_0(\vec{r}'-\vec{r}'')$$

$$t_R(\vec{r}'',\vec{r}) \, d\vec{r}'' \qquad (15)$$

where

$$G_0(\vec{r}) = 1/(8\pi^3) \int (\exp(i\vec{k}\cdot\vec{r})/E-\vec{k}^2+i\varepsilon)d\vec{k}$$

and ε = electron self energy and $G_0(r)$ is called the outgoing propagator. What is happening here is that $T(\vec{r})$ is being represented by the addition of a number of series summations where the first series summation represents all of the possible single scattering, the second series gives double scattering and so on.

Now the integrals are where the quantum mechanics comes in and these are solved by a series of manipulations which convert the plane waves to spherical waves. Variables are changed to eliminate the R dependence and then the $t(\vec{r})$ terms are expanded in an angular momentum

representation. This allows the angular integrations to be done since the radial part can be separated. Because the mathematics involved is rather lengthy,[10,11] only the result will be given

$$t_{R,\ell}(\vec{k}) = \int t_{R,\ell}(\vec{r}',\vec{r}) \sum_{j\ell} (\vec{k}\vec{r}') \sum_{j\ell} (\vec{k}\vec{r})\, \vec{r}^{\,2} d\vec{r}\, \vec{r}'^{\,2} d\vec{r}'$$

The expression for the intensity is now

$$I(\vec{k}\to\vec{k}') \propto \Big| \sum_{LL'} Y_L(\vec{k}')\, Y_{L'}(\vec{k}) \Big(\sum_{R} \exp(i(\vec{k}-\vec{k}')\cdot\vec{R})\, t_{R,\ell}(\vec{k})\, \delta_{L,L'} + \sum_{R\neq R'} \exp(i(\vec{k}\cdot\vec{R}-\vec{k}'\cdot\vec{R}'))\, t_{R,\ell}(\vec{k})\, G_{L,L'}(\vec{R}'-\vec{R})\, t_{R,\ell'}(\vec{k}) + \ldots \Big]\Big|^2 \tag{16}$$

where

$$G_{LL'}(\vec{r}) = \int G_0(\vec{y}-\vec{z}+\vec{R})\, i^{\ell'-1} \left(Y_{L(y)}\, Y_{L'(z)}\right) / \sum_{j\ell} (\vec{k}_y) \sum_{j\ell} (\vec{k}_z)\, d\vec{r}_y d\vec{r}_z$$

an angular integration over the propagator.

So far, we have considered each atom individually but to do the summations involved in Eq. (16) the symmetry of the crystal must now be considered. The crystal is divided into layers and each layer is then divided into subplanes so that each subplane has only one type of atom. All subplanes have an identical structure with one atom per unit cell. In this case an adsorbed layer on the surface would be treated just as some additional subplanes.

Now Eq. (16) is manipulated to do a summation over the subplanes with lattice vector $\vec{p}$ and reciprocal lattice vector $\vec{g}$. The scattering

matrix $t_{R,\ell}$ is computed for a plane v to give $t_v(\vec{k})$. The summation over $\vec{R}$ for $\vec{R}=\vec{R}_1$ becomes

$$\sum_{R_1,\ldots R_n} \exp(-i\vec{k}'\cdot\vec{R}_n + i\vec{k}\cdot\vec{R}_1)\; G_{LL'}(\vec{R}_n-\vec{R}_{n-1})\cdot G(\vec{R}_{n-1}-\vec{R}_{n-2})$$

$$\ldots\; G(\vec{R}_2 - \vec{R}_1) \;=$$

$$\sum_{R_1} \exp(i\vec{k}\cdot\vec{R}_1)\; G(\vec{R}_2-\vec{R}_1) = \exp(i\vec{k}\cdot\vec{R}_2) \sum_{p\neq 0} G(\vec{p})\exp(-i\vec{k}\cdot\vec{p})$$

$$= \exp(i\vec{k}\cdot\vec{R}_2)\; G^{sp}(\vec{k})$$

where G^{sp} is the propagator of the subplane assuming that $\vec{R}_2$ is in the same subplane as $\vec{R}_1$, if not the summation becomes

$$\sum_{R_1} \exp(i\vec{k}\cdot\vec{R}_1)\; G(\vec{R}_2-\vec{R}_1) = \exp(i\vec{k}\cdot\vec{R}_2) \sum_{p} G(\vec{p}+d\vec{v}_2-d\vec{v}_1)\cdot \exp(i\vec{k}(\vec{p}+d\vec{v}_2-d\vec{v}_1))$$

$$= \exp(i\vec{k}\cdot\vec{R}_2)\; G^{v_1 v_2}(\vec{k}) \qquad (17)$$

where $d\vec{v}_2$ is the position of any atom in plane two and the propagator $G^{v_1 v_2}(\vec{k})$ is independent of $\vec{R}$. So now the scattering matrix can be written as a function of propagators within the same subplane and between different subplanes independent of $\vec{R}$. This transformation is then done for the $\vec{R}_2$ sum and so on until the $\vec{R}_n$ sum. This becomes

$$\sum_{R_n} \exp[i(\vec{k}-\vec{k}')\cdot\vec{R}_n] = \sum_p \exp[i(\vec{k}-\vec{k}')\cdot(d\vec{v}_n+\vec{p})]$$

$$= \frac{(2\pi)^2}{A} \sum_g \delta(\vec{k}_{\parallel} - \vec{k}'_{\parallel} - \vec{g}) \exp[i(\vec{k}-\vec{k}')\cdot d\vec{v}_n]$$

where A is the area of the unit cell in the plane n, $\vec{k}_{\parallel}$ and $\vec{k}'_{\parallel}$ are the parallel components of $\vec{k}$, $\vec{k}'$. To get the total scattering we sum over all possible scattering paths within each subplane which we will designate as t_v' and then sum over all planes. So

$$t_v' = t_v(\vec{k}) + t_v(\vec{k})\ G^{sp}(\vec{k})\ tv(\vec{k}) + \ldots$$

$$= t_v(\vec{k})\ [1 - G^{sp}(\vec{k})\ t_v(\vec{k})]^{-1}$$

$$= (t_v^{-1}(\vec{k}) - G^{sp}(\vec{k}))^{-1} \quad . \tag{18}$$

Here $t_v(\vec{k})$ is the individual scattering matrix and can be determined by $\vec{k}$, the wave vector of the incident beam and $\delta_l(E)$ the phase shift computed from the scattering potential,

$$t_v^{-1}(E) = -m[g(E) - ik(E)]/2\pi\hbar^2 \quad g(E) = k(E)\cot[\delta_\ell(E)]$$

Summing over all planes, T_v is done as the sum over all paths which end in the subplane v so that the total scattering is the sum of the scattering in v plus the scattering in v after the electron has been

scattered from v'

$$T_v = t_v' + t_v' \sum_{v' \neq v} G^{vv'}(\vec{k})\, T_{v'}$$

Now substituting into Eq. (16) the intensity becomes

$$I(\vec{k} \to \vec{k}') \propto \Big| \sum_{LL'} Y_L(\vec{k}')\, Y_{L'}(\vec{k}) \Big[\sum_v \exp(i(\vec{k}-\vec{k}')d\vec{v}) T_v \Big]_{LL'}$$

$$\cdot \frac{(2\pi)^2}{A} \sum_g \delta(\vec{k}_{\parallel} - \vec{k}_{\parallel}' - \vec{g}) \Big|^2 \qquad (19)$$

So it would appear that we have a method for calculating intensities, but since Beeby has considered only elastic scattering and only about ten percent of the incident low energy electrons are back-scattered elastically, it is obvious that these intensities have little correlation with experiments.

Beeby's formalism essentially compacts the quantum mechanics involved in the scattering of an electron by a potential into $t_v(\vec{k}(E))$. It was noted that the inverse of the matrix $t_v(\vec{k}(E))$ could be computed from the incident wave vector and the phase shift. This calculation of the phase shift depends upon the V(R) used in the muffin-tin potential and so, choosing V(R) will play a great part in determining the intensities of the scattered beam. Pendry calculates the potential by neglecting screening, correlation, inelastic and incoherent processes since at higher energies these terms are relatively small.

The last two contributions are part of the imaginary component of the potential, which affects the calculated intensities markedly so this is a limitation which is rather important. The potential due to the Hartree term is evaluated exactly

$$V_H(\vec{r}) = -\frac{z}{|r|} + \sum_i \int \frac{|\psi_i(r_i)|^2}{|r-r_i|} \, d^3\vec{r}_i$$

but the exchange term is only approximate

$$V_{exch}\phi(\vec{r}) = \sum_i \int \frac{\psi_i(\vec{r})\psi_i^*(\vec{r}\,')\phi(\vec{r}\,')}{|r-r'|} \, d^3\vec{r}\,' \quad .$$

The exchange potential acting upon plane waves can be written as a summation over ℓ.[12] The summation is done until it converges (usually at $\ell = 4$) and the potential of the ion core is considered to be the sum of the Hartree and the exchange contributions.

Inelastic Scattering Model of Duke, Tucker, and Larramore

Duke and Tucker[13] showed that an inelastic collision model based on the strong electron-electron interactions of an energetic electron scattering in a solid limits the penetrating depth of the electron beam to about ten angstroms for electrons below 150 eV. They used a propagator formalism similiar to Beeby's and considered only S wave scattering, that is, the potential is assumed to scatter isotropically. The model is a system in which the ion cores of the lattice are surrounded by a uniform electric fluid which is bounded

by the potential of the outermost ion core. A propagator similiar to Beeby's is then defined with a damping parameter included which takes into account the inelastic scattering. $G_0(\vec{r},E)$ becomes

$$G_0(\vec{r},E) = \frac{-m}{2\pi\hbar^2} z(E) \frac{\exp[i\vec{k}_1(E)\vec{r}] \exp[-\vec{k}_2(E)\vec{r}]}{\vec{r}} \tag{20}$$

where the damping factor is $\exp(-\vec{k}_2(E)r)$, and $z(E)$ is a renormalization coefficient since the propagator was evaluated using the quasiparticle approximation from many-body collision theory.[14] The results of the damping is that the summations for $G^{vv'}$ and t_v' (Eqs. 17 and 18) converge more rapidly. Although this damping factor considers energy loss due to electron-electron coulombic interactions, there are other possible ways for the electron to be scattered inelastically. Bulk or surface plasmons may be excited and Duke and Tucker estimate that this may be a significant energy loss mechanism. However, if it was included, it would only add another damping factor to the propagator and so actually by careful choice of the damping parameter $\vec{k}_2(E)$, this deficiency is overcome.

It is a well known fact that the intensity of a diffracted beam changes as the temperature of the crystal is varied. This attenuation of intensity as the crystal temperature is increased is due to the increased displacement of the atoms from their mean positions because of greater vibrations and is called the Debye-Waller factor. Using a Debye model for the phonon spectrum of the solid Larrimore and Duke

derived a Debye-Waller factor within the propagator formalism.[14] They assume that only the surface layer of the crystal will be displaced and so distinguish between the scattering amplitude of the surface and the bulk by using a different phase shift for the individual scattering matrix t.

$$t_S^\circ(|\vec{k}(E)|) = \frac{\pi i\hbar^2}{m|k(E)|}\,[\exp(2i\delta_S)-1]$$

$$t_B^\circ(|k(E)|) = \frac{\pi i\hbar^2}{m|k(E)|}\,[\exp(2i\delta_B)-1]$$

Now an effective scattering matrix with a Debye-Waller factor is defined for each plane v.

$$b_v(\vec{k},\vec{k}',E_i) = \exp[-W_v(\vec{k}'-\vec{k})]\; t_v(\vec{k}',\vec{k},E_i) \tag{21}$$

But from the Debye model[14]

$$W_v(\vec{k}'-\vec{k}) = \frac{3t^2(\vec{k}'-\vec{k})^2}{2Mk_B\Theta_D v}\left[\frac{1}{4}+\left(\frac{I}{\Theta_D\lambda}\right)^2\int_0^{\Theta_D\lambda/T} x\,dx/e^x-1\right]$$

when $\exp(-W_v(\vec{k}'-\vec{k}))$ now depends upon angular momentum ℓ where b_v is expanded in terms of partial waves. Larramore and Duke do the expansion using s and p waves to compute the effective scattering matrix and get

$$b_v^L[\vec{k}(E)] = t_v(\vec{k}(E))\,\exp(-2wk^2(E))\;4\pi S_0\,|\vec{k}(E)| \quad \text{for } L=0$$

$$b_v^L(\vec{k}(E)) = t_v(\vec{k}(E))\,\exp(-2wk^2(E))\;4/3\;\pi S_1\,|\vec{k}(E)| \quad \text{for } L=1$$

where $$w = W_v(\vec{k}'-\vec{k})$$

$$S_0(\vec{k}(E)) = \sinh 2wk^2(E)/2wk^2(E)$$

$$S_1(\vec{k}(E)) = [3/2\ wk^2(E)][\cosh(2wk^2(E)) - \sinh 2wk^2(E)]/2wk^2(E)$$

Now b_v^L can be used to get the scattering in a plane t_v' as before (Eq. 18). The intensities calculated by both the inelastic damping factor and the Debye-Waller factor would be expected to correlate much more readily with the experimental ones. Because it has become apparent that S wave scattering is not a very good approximation of the actual scattering amplitudes, Duke, Tucker, and Larramore have modified their program so that a number of phase shifts can be included in a computation taking a reasonable amount of time by using a perturbation approach to calculating the T matrix.

Tong and Rhodin's Program

Tong and Rhodin also use a scattering propagator method based upon Beeby's formalism. They modified the inelastic scattering of Duke and Tucker by including higher order phase shifts calculated from Pendry's potentials using the muffin tin approximation. Besides the inelastic damping factor they include an explicit term for the damping due to single particle and bulk plasmon excitations based upon the self energies of an interacting, homogeneous electron gas.[15]

The Debye-Waller factor that they use is similiar to Duke's treatment. The main innovation of their program was the development of a perturbation approach to the calculation of the t_v matrix. The total scattering matrix is presented as

$$[T_v]_{\ell\ell'} = (t_v)_\ell \, \delta_{\ell\ell'} + \sum_{\ell''} (t_v)_\ell \sum_{v=0}^{\infty} [G^{vv'}]_{\ell\ell'} (T_{v'})_{\ell'\ell''} \qquad (22)$$

where $t_{v,\ell} \, \delta_{\ell\ell'}$ is the diagonal individual scattering matrix in plane v. Equation (22) is iterated in terms of $(t_v)_\ell \, \delta_{\ell\ell'}$ to third order instead of getting $(t'_v)_\ell$ from a matrix inversion. The summation is done over all terms in the scattering in one plane and scattering between planes. The summation over the lattice can be transformed into sums involving the reciprocal lattice vectors and for the third order summation this gives only three possible terms. This makes a tremendous difference in computer time and the error introduced is minimal for nearly normal incidence. The convergence of the perturbation method was checked by calculating $(t'_v)_{\ell\ell'}$ to infinite order using the usual matrix inversion and comparing it to the third order perturbation result and was found to agree quite closely.

Martin and Somorjai's Program

A computer program[16] has been constructed by Martin using Beeby's formalism and it is similiar to the approaches already discussed. The inelastic damping factor originated by Duke and Tucker is used and a Debye-Waller factor is also included. Using a perturbative approach similiar to Tong and Rhodin's, t matrix inversion is avoided and so

the program can use a number of phase shifts without long calculation times. Pendry's program for the calculation of phase shifts of the potentials is used. The inner potential can be calculated using either a Lundqvist or Optical model. The inner potential is a term used to describe the increase in kinetic energy that the electron in vacuum gains upon entering a metal. Three separate effects can be distinguished. The first is the difference in potential between an electron outside the surface in vacuum and the Fermi level. This is called the work function and can be considered due to the fact that the electron wavefunctions extend a short distance outside the surface layer. The second effect is the presence of positively charged ion cores in the crystal which are only partially screened by the electrons in the conduction and valence bands. This screening is the third effect and it depends upon both the electron density and the momentum of the incident electron. The incident electron surrounded by screening electrons can be thought of as a quasiparticle.[17] The quasiparticle energy can be written as the energy of the free electron with wave-vector $\vec{k}$ plus a complex self energy correction $\Sigma(\vec{k},E)$. The imaginary part of the quasiparticle energy $-\Sigma_2(\vec{k},E)$ is directly related to the damping factor $-\vec{k}_2(E)$ of Duke, Tucker, and Larramore. The Lundqvist model calculates the self energy correction as a function of incident electron energy by assuming that the metal is a uniform electron gas with a given density supplied as a parameter. The optical model assumes that the real and imaginary part of the self energy correction are essentially constant over the experimental range of incident

electron energy and treats these constants as adjustable parameters.

Pendry's Wave Matching Method

The seconds general approach to the LEED scattering problem uses the differential form of the Schroedinger equation to solve for the scattering within the crystal in terms of Block waves and then matches these to the wave functions outside of the crystal. The crystal is assumed to be infinitely perfect with a surface layer that may be displaced. The displaced surface layer is treated separately as a slab of the perfect crystal that has been shifted and so the wave function must be matched at the boundary between the surface and the perfect crystal and at the surface-vacuum boundary.

It is assumed that the Block waves of the infinite crystal are known and can be written in terms of the incident wave vector $\vec{k}$ and the reciprocal lattice vector $\vec{g}$.[20] There will be an infinite number of Block waves having a component of the incident wave vector parallel to the surface of the crystal but we look at 2n waves having Fourier components parallel to the surface. They can be written in the form

$$\psi_{k_i}(\vec{R}) = \sum_{i=1}^{n} F_{ij} \exp((\vec{k}_i + \vec{g}_i)\cdot\vec{R})$$

where n is the number of reciprocal lattice vectors. Now the shift of the surface layer ab is along the z axis and it is displaced a distance c-b. We can write the expression for a plane wave outside the crystal:

$$\phi_i = \exp[i(\vec{k}_i\vec{z} + (\vec{k}_{\parallel} + \vec{g}_{\parallel_i})\cdot\vec{R})]$$

where $\vec{k}_{\parallel}$ is the component to k parallel to the surface, $\vec{g}_{\parallel_i}$ is the parallel of the reciprocal lattice vector and

$$\vec{k}_i = \pm (2E - |\vec{k}_{\parallel} + \vec{g}_{\parallel_i}|^2)^{1/2}$$

Now the wave function in the four regions is written as

$$z > a \quad \psi(x,y,z) = \sum_{i=1}^{2n} P_i \phi_i \ (x,y,z-a) \tag{11}$$

$$b > z \quad \psi(x,y,z) = \sum_{i=1}^{2n} Q_i \psi_{ki}(x,y,z-a)$$

$$c > z > b \quad \psi(x,y,z) = \sum_{i=1}^{2n} S_i \phi_i \ (x,y,z-b)$$

$$z > c \quad \psi(x,y,z) = \sum_{i=1}^{2n} T_i \psi_{ki}(x,y,z-c)$$

The summation is over 2n waves with the first set of n components propagating in the plus z direction and the second set in the minus z direction, e.g. for region 1, the sets give the components P^+ and P^- where P^- are the amplitudes of the reflected waves. At z=a, the two wave functions and their derivatives are matched and these can be written as a matrix

$$\sum_{i=1}^{2n} A_{ij}{}^{\circ}(0) P_j = \sum_{j=1}^{2n} A_{ij} \ (0) Q_j$$

where $A_{ij}(0)$ is a 2n×2n matrix which when acting on P_j generates the n Fourier components parallel to the surface at z=a for the first n rows. The second n rows of $A_{ij}(0)$ acting on P_j find the n Fourier

components of the first derivative.

The A matrix is then written for the other two boundaries in the same way

$$z = b \quad \sum_j A_{ij}(b-a)\, Q_j = \sum_j A_{ij}{}^{\circ}(0) S_i$$

$$z = c \quad \sum_j A_{ij}(c-b)\, g_i = \sum_j A_{ij}{}^{\circ}(0) T_j$$

To actually perform the calculation, the matrices A_{ij} are rewritten in terms of matrices using Bloch waves

$$A(z) = \left[\begin{array}{c|c} B+(z) & B-(z) \\ \hline B+'(z) & B'-(z) \end{array}\right]$$

where

$$B_{+ij}(z) = \sum_{j,r} F_{j,r} \exp[i(\vec{k}_{\perp i} + \vec{g}_{\perp r})\vec{z}]$$

These three matrix equations are then solved for P^- in terms of P^+. Knowing P^- the wave function for the electrons being reflected back from the surface of the crystal can be calculated from Eq. (11). The wave function is really a probability amplitude so it determines the intensities calculated. This particular treatment applies to elastic scattering but it indicates the general direction of the method. The formalism appears simple but all of the scattering problems are inherent in the calculation of the Bloch waves and the matrices. To do this one needs to calculate the band structure of the crystal and uses a pseudopotential in determing the Bloch waves. Pendry has used this

formalism to consider an inelastic scattering model and has said that it simplifies the matrix calculations. He uses an imaginary component of the potential in calculating the wave function. He then shows that the matrix elements for backwards scattering are much smaller than the inelastic terms which are approximately equal to or less than the forward scattering.[18] He therefore assumes that since most of the scattering is in the forward direction one need only do multiple scattering for these terms, the intensities of the backward scattered beams are sufficiently small so that they can be calculated as a perturbation. The wave function within the crystal is calculated using Bloch waves and expanding in terms of the forward scattered waves.

$$|\psi_k\rangle = \sum_g a_{\vec{g}}(\vec{k}) \; |\vec{k} + \vec{g}\rangle \tag{12}$$

The coefficients a_g are used to get the matrix M containing all forward scattered waves

$$\sum_g (\tfrac{1}{2}|k+g|^2 - E)\delta_{gg'} + \langle k+g \; |V+iVj| \; k+g'\rangle) \; a_{g'}(\vec{k}) = \sum_{g'} M_{gg'}(\vec{k}) q_g(\vec{k}) = 0$$

the matrix elements for forward waves, V_f, are

$$V_f \gg (\tfrac{1}{2}\,|k|^2 - \tfrac{1}{2}\,|k+g|^2)^2 + V_i^{\,2}$$

The wave function at the surface is found by a summation of the Bloch waves, $|\psi_{\vec{k}_i}{}^A\rangle$ and Eq. (12)

$$|\psi\rangle = \sum_{k_i} c(\vec{k}_i)\ |\psi_{k_i}{}^A\rangle$$

$$= \sum_{k_i} \sum_{g} c(\vec{k}_i) b_{g_i}(\vec{k}_i)\ |\vec{k}_i + \vec{g}\rangle$$

This wave function has been matched at the surface for the backward travelling w waves which are found using the proper terms for the coefficients.

Because these calculations are rather long, Pendry has developed the perturbation approach to get the wave function. The wave function between layers h and (h-1) is written as a sum of plane waves in the (± z) directions

$$\psi = \sum_{g} (U^+_{hg} \exp[i\vec{k}^+_g \cdot (\vec{r}-h\vec{a})] + U^-_{hg} \exp$$

$$[i\vec{k}^-_g \cdot (\vec{r} - h\vec{a})]$$

where $\vec{k}_g^{\pm} = \pm(2E-2V_o-\vec{k}_{g_x}^2 - \vec{k}_{g_y}^2)^{1/2}, \vec{k}_{ox} + \vec{g}_x, \vec{k}_{oy} + \vec{g}_y)$

$\vec{a}$ = displacement of layer h from layer (h-1)

$\vec{k}_{ox}$ and $\vec{k}_{oy}$ are components of incident wave vector parallel to the surface

V^+ is the amplitude of the forward wave, V^- is backward. A propagator for forward waves between h and (h-1) is defined

$$P^{+}_{gg'}(j-h) = \exp[i\vec{k}^{+} \cdot (j-h)\vec{a}]\delta_{gg'}$$

so without any scattering $U^{+}_{hg} \rightarrow U^{+}_{jg}$ as the wave propagates to between the j and (j-1) layers

$$\sum_{g} U^{+}_{ig} \exp[i\vec{k}_{g}^{+} \cdot (\vec{r}-j\vec{a})] = \sum_{g}\sum_{g'} P^{+}_{gg'}(j-h)U^{+}_{hg} \exp[i\vec{k}^{+}_{g} \cdot (\vec{r}-j\vec{a})]$$

If forward scattering is strong, the amplitude U_{jg} is not just the propagation from U_{hg} but must include scattering from between other layers, so that the wave may be propagated from h to k by $P^{+}(k-h)$ and then forward scattered and then propagated to other layers where the scattering is represented by M^{+}. So a new propagator which contains all possible forward scattering processes which might contribute to the forward propagation of the wave from h to j is now defined as the renormalized forward-scattering propagator.

$$P^{+}_{RFS}(j-h) = P^{+}(j-h) + \sum_{L\leq k\leq j} P^{+}(j-\vec{k})M^{+}P(\vec{k}-L) + \sum_{L\leq k\leq \ell < j} P(\overleftarrow{j}-\ell)M^{+}P^{+}(\ell-k) \tag{13}$$

$$M^{+}P^{+}(k-h) + \ldots$$

Using

$$P^{+}(j-h) = [P^{+}(1)]^{j-h}$$

Then

$$P^{+}_{RFS}(j-h) = [P^{+}(1)(1+M^{+})]^{j-h} \tag{14}$$

Now a perturbation series similar to Eq. (14) is written for back-scattering using M^{-} and a renormalized propagator for propagation out of the crystal from layer h

$$P^-_{RFS}(j-h) = [(1+M^+)P^-(1)]^{j-h}$$

With this, the amplitude for back scattering is calculated for the first order

$$V^-_o \sum_h P^-_{RFS}(h)M^- P^+_{RFS}(h)V^+_o$$

Apparently this series converges rapidly so that the first and third order summations are sufficient to give excellent agreement with the exact results.

Korringa-Kohn-Rostocker Method used by Jepsen, Marcus and Jona

Jepsen and Marcus use a method which is a curious combination of both of the approaches we have discussed, the scattering propagator and the expansion into Bloch waves, in order to obtain the wave function within the crystal.[19] The principles involved in the formalism have essentially been covered in the preceeding discussion. The program contains an inelastic damping factor using Snow's potentials derived from band structure calculations. A Debye-Waller factor similiar to Duke and Larramore's is used.

Applications to Structure Analysis

We have considered a number of approaches to LEED intensity theory since all are based on a quantum mechanical description of the scattering process, they should give the same results providing that the model upon which they are based is a realistic one. However, since the ultimate goal is structure analysis, it is important to

consider whether any method enjoys some advantage over the others. In looking at surface structures it is immediately obvious that one is interested in investigating adsorbed atoms or molecules on the surface. This means that the surface will almost always be quite different from the next two or three layers of the crystal and in the case of the adsorption of complex molecules, the adsorbed layer itself may have to be considered as several layers. Of the two general approaches, the propagator method derived by Beeby is much more suited to this situation since it automatically considers each layer separately and so makes no assumptions about the symmetry of the crystal. In contrast, the approach used by Pendry considers the entire crystal to be entirely symmetric and then the surface layer must be treated separately as a thin slab sitting on the crystal. With complex adsorption layers, it may become difficult to match the wave functions of the various regions at the boundaries since the question of where the potential of the substrate stops and the adsorbed layer starts becomes very complex. All of the programs consider inelastic scattering by including some kind of damping factor, all can include variation in the incident beam angle, and all have some sort of Debye-Waller factor. Given a sufficient number of phase shifts, all the methods considered are capable of producing intensity curves which agree with the experiment for simple metals where the potential is known. All consider the positions of the atoms on the surface in their calculations and appear to be sensitive enough to determine the surface position uniquely.

C. Surface Structure Nomenclature

Because most of the existing work done with LEED consists of observing the diffraction pattern formed during various stages of the experiment, a special terminology has developed to characterize these patterns conveniently.[21] The unit cell of the surface structure formed is described in terms of the bulk unit cell as determined by X-ray diffraction. If the arrangement of atoms on a crystal's surface is identical with the bulk unit cell, the structure formed is called a (1×1). In the case of a clean metal, this would be considered the substrate structure, if the surface was an overlayer formed by deposition or adsorption, the pattern would be indexed as a (1×1)-x structure where x is the atom or molecule that makes up the surface. Often the diffraction patterns observed have unit cells that are integral multiples of the substrate structure. For example, if the lattice vector of the surface structure is twice as long as that of the bulk cell in one direction and the same as the bulk in the other, the surface structure would be designated a (2×1). Examples of some diffraction patterns and their equivalent real space lattices designated in this way are given in Figs. II-2 and II-3.

More complicated diffraction patterns can sometimes by considered as resulting from surface structures with unit cells that are non-integer multiples of the bulk unit cell and rotated with respect to the bulk. The second pattern in Fig. II-4 shows the $(\sqrt{3} \times \sqrt{3})$ - R 30° which occurs if every third lattice site along a row of the hexagonal

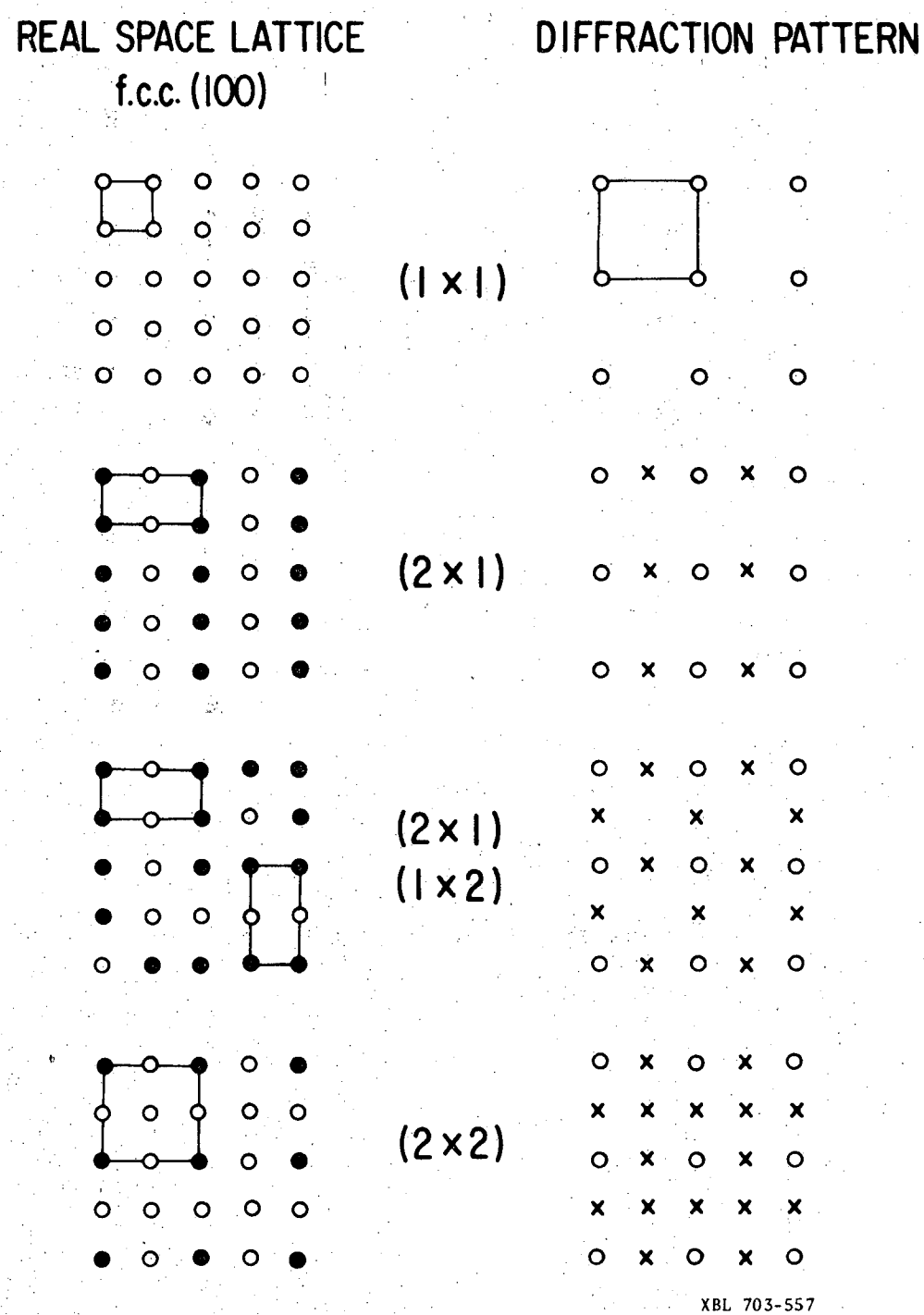

Fig. II-2. Real space lattices and diffraction patterns; x's in diffraction patterns are extra features caused by surface structures.

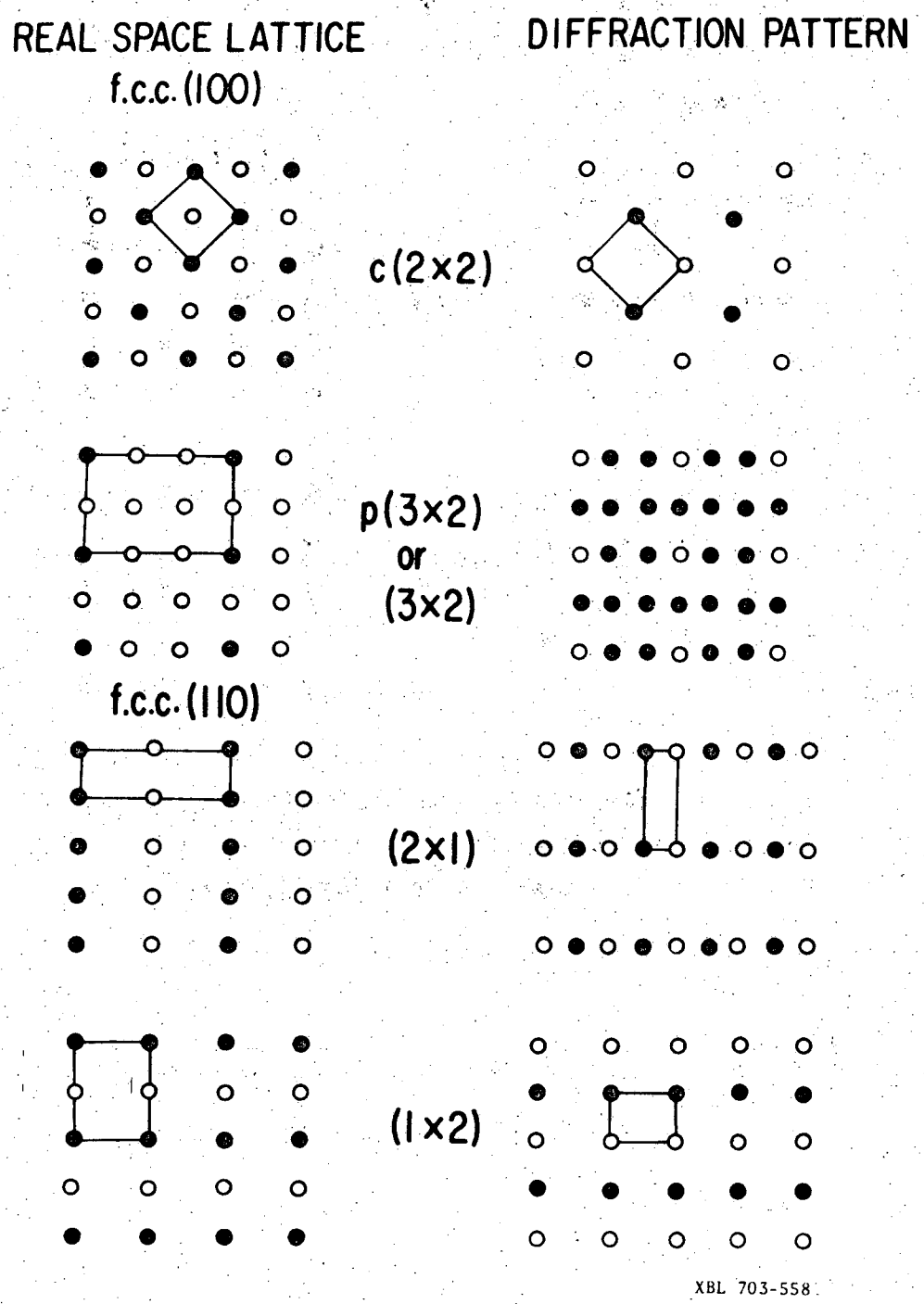

Fig. II-3. Real space lattice and diffraction patterns; x's in diffraction patterns are extra features caused by surface structures.

0 0 0 0 3 9 0 0 7 0 9

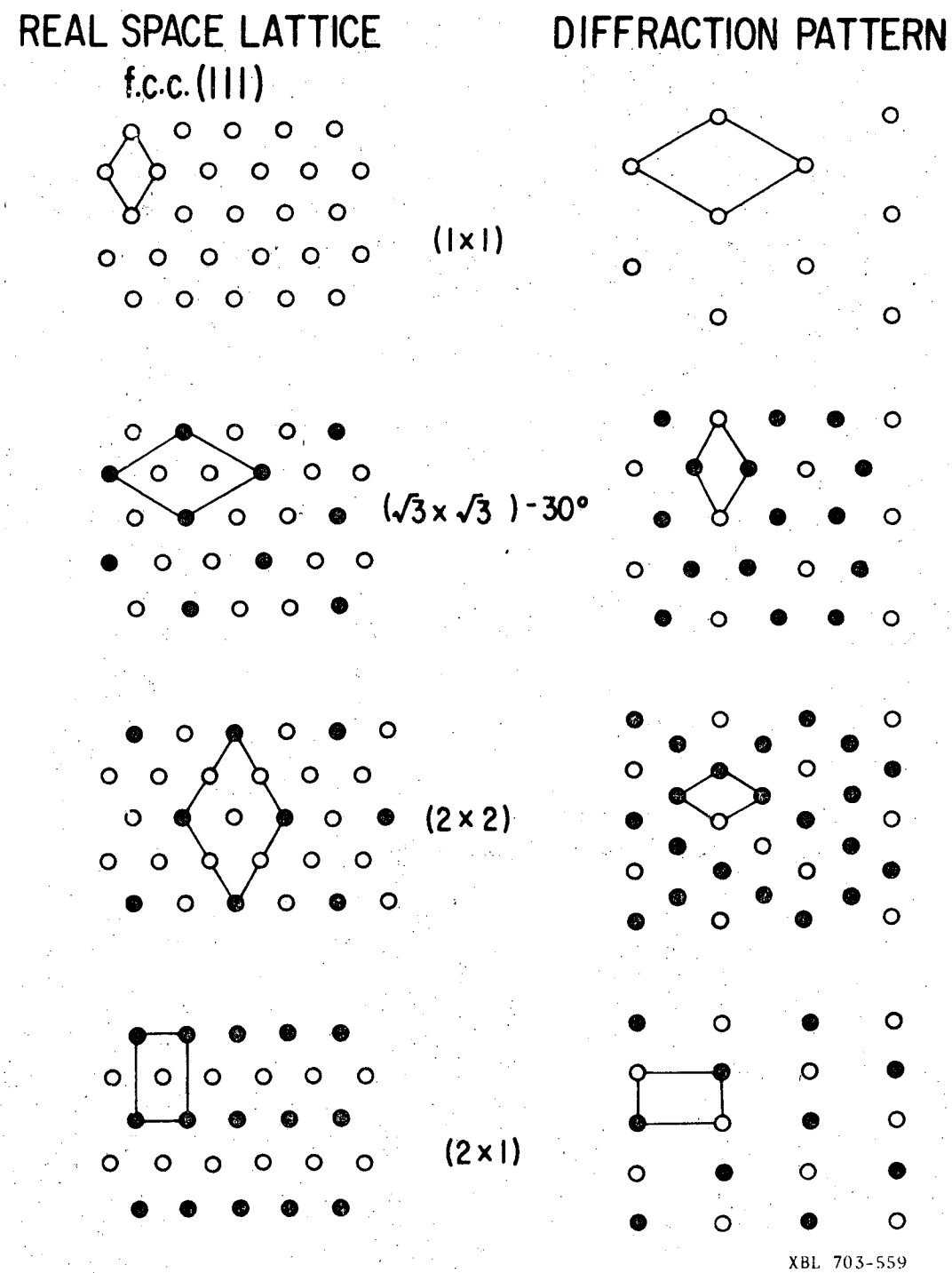

Fig. II-4. Real space lattices and diffraction patterns; x's in diffraction patterns are extra features caused by surface structures.

lattice is occupied. If this method does not work, a matrix notation can be used to describe the primitive translation vectors of the surface net in terms of the translation vectors of the substrate, $\vec{a}$ and $\vec{b}$. For instance, the translation vectors of the $(\sqrt{3} \times \sqrt{3})$-R30° structure would be $\vec{p} = \vec{a} + 2\vec{b}$ and $\vec{q} = 2\vec{a} + \vec{b}$ and the matrix which describes the structure is

$$\begin{pmatrix} 1 & 2 \\ 2 & 1 \end{pmatrix} .$$

In general, if $\vec{p} = a_1\vec{a} + b_1\vec{b}$ and $q = a_2\vec{a} + b_2\vec{b}$ the matrix is

$$\begin{pmatrix} a_1 & b_1 \\ a_2 & b_2 \end{pmatrix} .$$

III. EXPERIMENTAL

A. Apparatus

A modified Varian LEED apparatus was employed in this project. The stainless steel diffraction chamber was connected to an Ultek 200 liter per second ionization pump via a gate valve. The system was also equipped with a water-cooled titanium sublimation pump and an auxiliary 50 liter/second Vacion pump. Two cyrogenic pumps containing a molecular sieve chilled to liquid nitrogen temperature accomplished the forepumping from atmosphere to pressures of about one micron. Gases could be admitted into the system through a capillary needle that was positioned approximately one centimeter from the sample with the rate of gas flow controlled by a Varian adjustable leak valve. Typical base pressures after bakeout were in the 10^{-10} Torr range and all experiments on clean metal surfaces were done at 2×10^{-10} Torr.

The system had a Varian four-grid LEED optics which uses the post-acceleration technique to display the diffraction pattern on a fluorescent screen as shown in Fig. III-1. The electron beam is supplied by a bariated nickel cathode which is indirectly heated by an alumina-coated tungsten filament. An electrostatic lens focuses the beam which can have a voltage of 10 to 500 volts relative to ground with a nominal dispersion of .2 volts. The grid assembly allows only the elastically scattered electrons to penetrate and then be accelerated towards the fluorescent screen by a positive 5000 volt potential. To do this, the first grid is grounded to maintain the

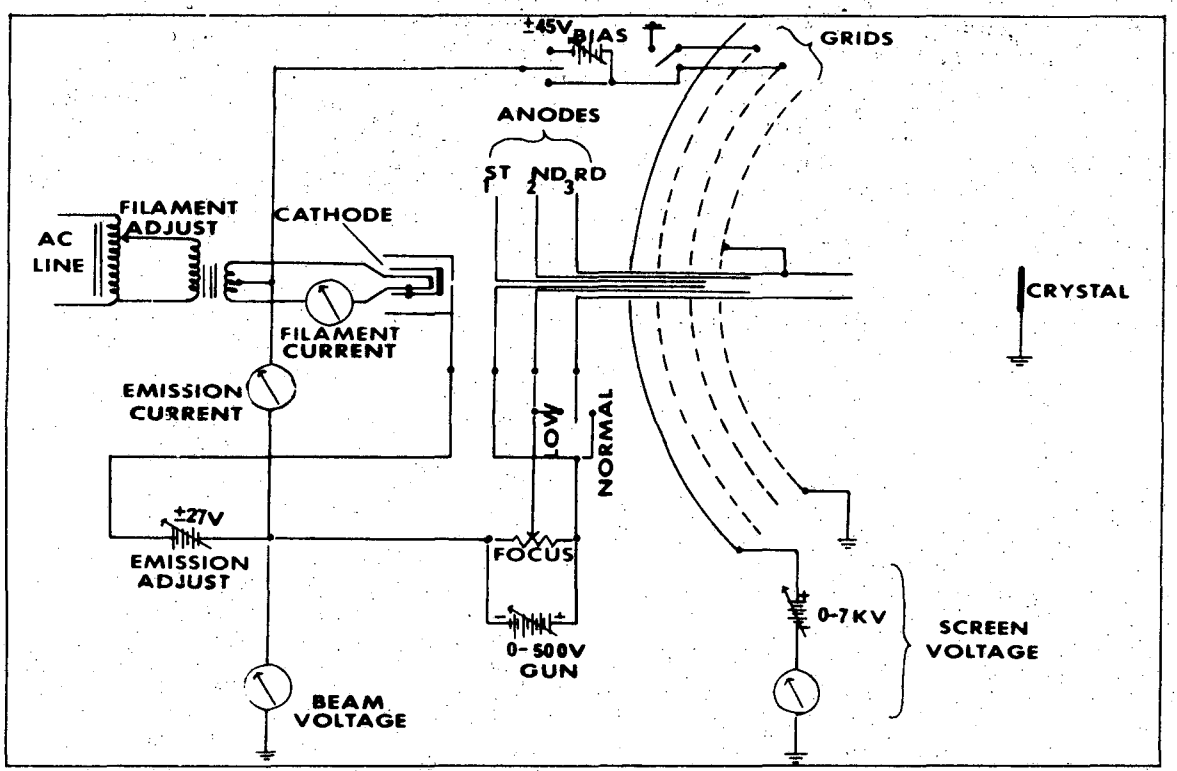

XBL 696-632

Fig. III-1. Schematic of LEED electron optics.

field free region around the sample. The second and third grids are coupled and at the cathode potential, thus they repell electrons that have been scattered inelastically. Because of the large positive potential on the screen however, not all inelastic electrons are repelled and so the fourth grid is used to improve resolution. It can be maintained at + 27 to - 27 volts with respect to the cathode potential. The grids are constructed of nickel plated tungsten and have a transparency of 80% each. Upon penetrating the grids the elastic electrons are accelerated onto the screen where their energy is converted to light by a phosphor. Within the ranges of current used in these experiments the intensity of the emitted light was a linear function of the current density[22] and it was this light intensity that was measured by a telephotometer or a photographic technique.

The samples were spot welded to polycrystalline platinum strips of 99.99% purity to avoid possible contamination problems. The (100) and (111) faces of platinum were mounted back to back on separate platinum strips. The strips were supported by two stainless steel pressure clamps which were bolted onto a ceramic block so that the samples were electrically isolated from the system. The ceramic was mounted onto the shaft of a Varian crystal manipulator with electrical feedthroughs that had been modified to eliminate precession of the shaft as it was rotated. The manipulator was connected to its flange by a stainless steel knife edge bellows so that it allowed translation of the samples in a direction parallel to the shaft, rotation about the axis of the shaft and movement in the x and y directions. The

crystal facing the electron gun was aligned so that it remained in the center of curvature of the screen through all rotation angles. High purity oxygen free copper braid wire was used to connect the sample supports with the electrical feedthroughs. The samples were resistively heated by passing an AC current of approximately fifty amperes through it. The sample holder was made so that the samples were the hottest points of the assembly and their temperature was monitored by a calibrated optical pyrometer.

B. Samples and Sample Treatment

The samples used in this research were single crystals of nominal 99.99+% purity platinum obtained from the Material Research Corporation in Orangeburg, New York. The platinum bar was electron beam zone refined and the major contaminants as determined by a spark source mass spectrometer were: Ge(30 ppm), Rh(15 ppm), C(10 ppm), Al(7 ppm), Si(7 ppm), W(5 ppm), Zr(2.5 ppm), Cr(2.5 ppm), Ti(2.5 ppm), Ni(2.5 ppm), Nb(1 ppm), Pd(.6 ppm), and Mn(.6 ppm).

The single crystal bar was oriented to within .5° of the desired face using Lave back reflection photographs and then spark cut. The samples were then mechanically polished with a series of progressively finer mesh abrasives and finally with .5 micron alumina powder. Next a solution of aqua regia at 100°C was used to etch the crystals. The etching treatment with a 50% aqua regia solution was repeated immediately before replacing the manipulator.

The cleaning of platinum has been thoroughly described.[23] The major problem in cleaning is carbon since it readily diffuses through the platinum lattice at higher temperatures. To clean new crystals cycles of ion bombardment followed by high temperature annealing followed by oxygen treatments were performed. The crystal surface was sputtered with 300 volt argon ions at pressures of argon that ranged from 5 to 8×10^{-5} Torr. This resulted in a current density at the crystal surface on the order of 6 microamps/cm^2. Annealing usually took place at 900°C and was followed by exposure to oxygen at a pressure of 1×10^{-5} Torr. Each new crystal received a total of about five hours of ion bombardment and twenty hours of oxygen treatment.

Subsequently the crystal at 900°C was treated for 30 minutes with oxygen at a pressure of 1×10^{-5} Torr to clean the surface before an experiment.

Unfortunately, the equipment necessary for Auger Electron Spectroscopy was not generally available for use in this research. However, an Auger unit was used to monitor the state of the surface during the time new samples were being cleaned. Figure III-2 shows examples of Auger spectra from the crystal with carbon and carbon monoxide still present after one of the initial cleaning cycles and from the clean surface after the complete treatment. Suggested transitions for the indicated Pt, C, and O peaks are also listed. All of the work on clean metal surfaces was done before the system was again exposed to atmosphere. Since the titanium sublimation pump has a high pumping speed for CO and the base pressure of the system was

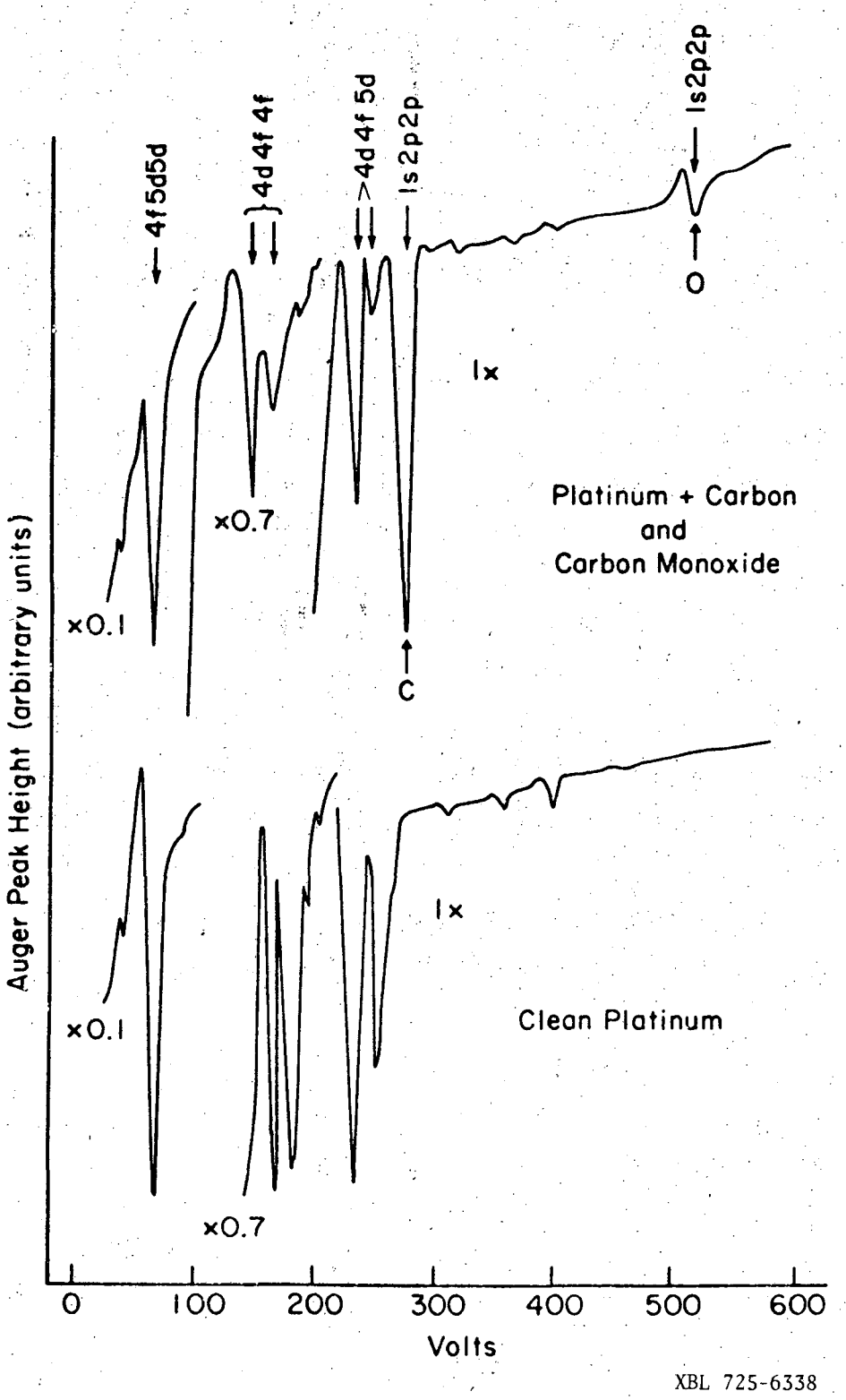

Fig. III-2. Auger spectra of platinum with carbon impurities and clean platinum.

2×10^{-10} it is unlikely that there was much CO in the ambient. Furthermore, the 5×1 pattern of the (100) face of platinum has proven to be extremely sensitive to carbon monoxide adsorption or the presence of carbon changing to a 1×1 unit cell. At no time did this happen during the study of the metal surfaces. Since the crystals were regularly treated with oxygen after a reasonable working time it can safely be assumed that the surfaces were clean when experiments were being performed.

C. General Experimental Procedure

Whenever the system had to be exposed to atmosphere either to insert the crystal samples or to make some modification of the apparatus all attempts were made to avoid contaminants or the adsorption of water vapor. The electron gun was shut off and allowed to cool for one hour before bringing the diffraction chamber up to atmospheric pressure with dry nitrogen through the roughing manifold. When the necessary work was completed and all the flanges had been resealed, the system was pumped down to a pressure of one micron by the two liquid nitrogen cooled roughing pumps. The ion pumps were started and when the pressure at the ionization gauge was in the 10^{-7} Torr range the system was prepared for bakeout. After baking out both the diffraction chamber and the ionization pumps at 140° for 12 to 24 hours, the shroud was removed. While the chamber was still hot the crystals, the titanium sublimation pump, the LEED gun, and the ion bombardment gun were all degassed. The samples were then ion bombarded, annealed, and oxygen treated until well ordered diffraction patterns and clean

surfaces were obtained. Before each experiment the titanium sublimation pump was run for a few minutes to maximize removal of CO and then an oxygen treatment was begun. After stopping the oxygen, heating of the crystals continued while the electron guns and sublimation pump were degassed. The crystals were then cooled for one hour as the pressure dropped from 10^{-9} to 2×10^{-10} Torr and the experiment was begun.

D. Intensity Measurement Techniques

1. Preliminary Considerations

Once the crystal had been cleaned and a good diffraction pattern had been obtained, measurement of the intensities of the beams could be started. However, since the electron gun used in these experiments did not provide constant beam current as the beam voltage was changed, a calibration curve for incident beam current had to be constructed. The LEED optics power supply is equipped with a meter that measures the emission current from the cathode. This is assumed to be proportional to the beam current that emerges from the gun after passing through the electrostatic focusing system. To obtain a calibration curve for the fifty microamp emission current meter, current through the crystal and current to the screen were measured as a function of emission current for each crystal used. Current through the crystal was measured with the crystal at ground potential by a Keithley Electrometer Model 610B. Then the grid assembly was grounded and with a 200 volt applied potential on the screen its current was also measured by the electrometer. The two curves were added to obtain a

plot of incident beam current as a function of emission current which could be read to a .1 of a microamp and is shown in Fig. III-3. Because the grid system does not possess 100% transmittance and since the screen does not subtend a full 180° around the crystal not all of the backscattered current was measured but this error is certainly not more than 10% of the total beam current. Its effect is essentially cancelled out since the same limitations apply to the elastically scattered electrons during the LEED experiment.

Because scattered intensities are known to vary for changes in angle of incidence, the magnetic field in the region between the sample and the optics had to be reduced to a minimum. As the electron beam voltage is increased, the degree of deflection by the field decreases due to the difference in electron energy. Thus, in a magnetic field the angle of incidence of the electron beam changes with voltage. Field free conditions are obtained by bucking the magnetic field due to the earth and the magnets of the ion pumps by a small trimming magnet. By taking advantage of the crystal's symmetry at normal incidence, the trimming magnet can be adjusted until the degeneracy of the diffraction pattern is maintained over a two hundred volt range. It is then assumed that the beam is at normal incidence and the net magnetic field zero. Without a doubt this is the most frustrating part of the experiment and there are many times when one wishes that magnetic fields simply did not exist.

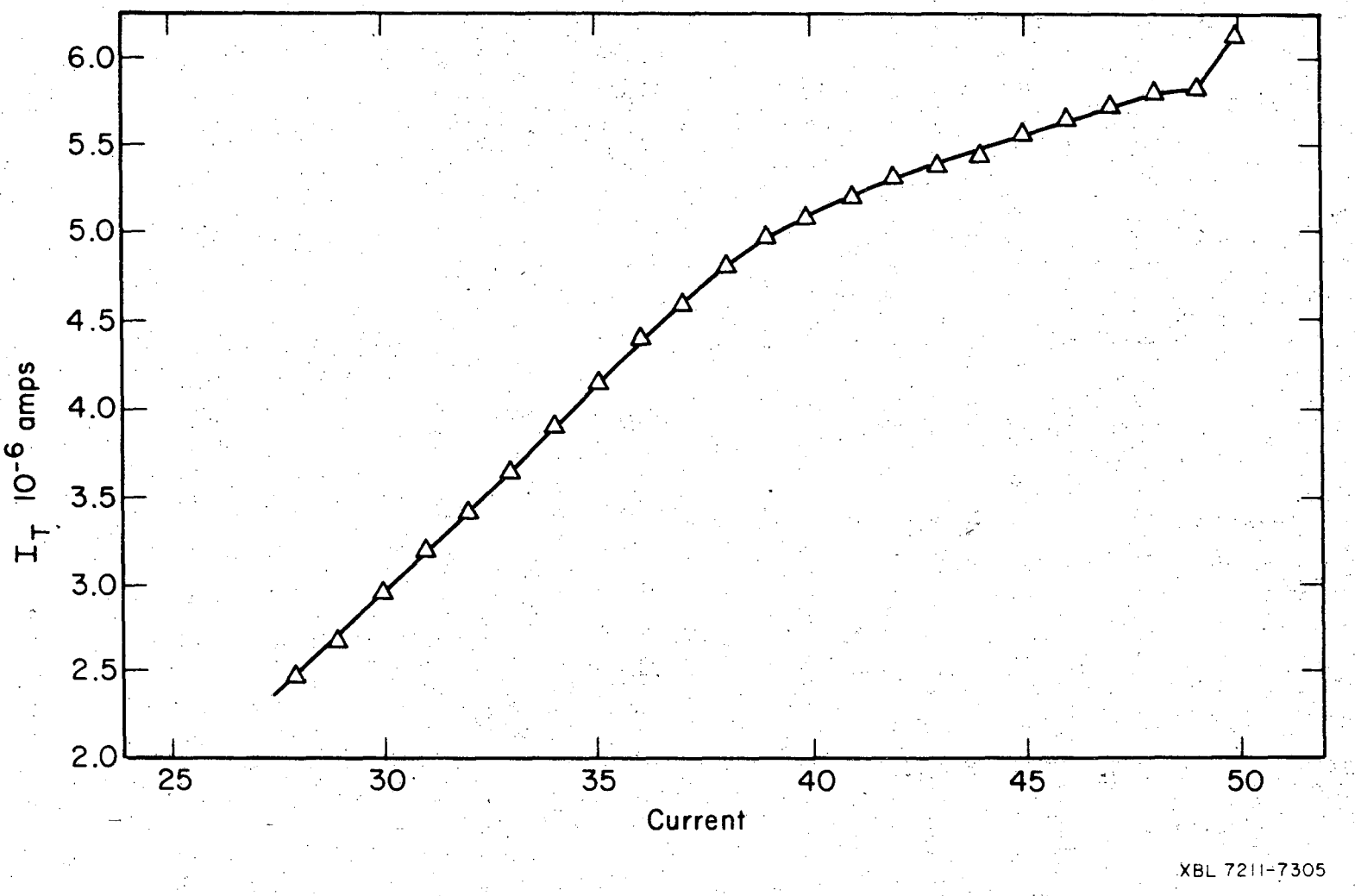

Fig. III-3. Total current versus emission current for Pt(111).

2. Spot Photometer

A spot photometer is the usual instrument used to measure intensities in a LEED apparatus of the post acceleration fluorescent display type. The photometer provides a direct measure of the spot's light intensity which is proportional to the current density of the diffracted beam. A Faraday cup collector can be used to measure the incident electron flux at a spot on the screen and thus calibrate the photometer to measure absolute intensities. For the specular (00) spot the scattering vector is perpendicular to the surface plane at all energies. Since the angle of the scattered beam is always equal to the incidence angle, the photometer can be focused on the stationary spot and a scan of intensity versus beam voltage can be made. If the emission current at each voltage is recorded it can be used to calculate the incident beam current from the calibration curve and the spot intensities can then be normalized. Unfortunately, the positions of the other diffraction spots does change with beam voltage and so the photometer must be moved and refocused for each change in voltage (no wonder most intensity work in the literature is for the (00) beam!). This complicates the matter a great deal since at 10^{-10} Torr one has about two and a half hours of working time before a clean surface is covered by a monolayer of gas (assuming that every molecule that hits the surface adsorbs). Thus the crystal must be cleaned a number of times before the intensities of all the beams are measured and for a complicated diffraction pattern this can increase the experimental time enormously.

In this project a telephotometer, Model 2000, from Gamma Scientific Incorporated was used to measure the intensities of the (00) beams. The optical head is constructed with a system of glass fibers and prisms between the objective lens system and the photomultiplier tube so that only the light transmitted by the fiber at the center of the image plane of the objective reaches the photomultiplier tube. One can choose an aperture defining 2, 6, 20, 60 or 180 minutes of arc. The focusing eyepiece is set up so that the fiber is seen in the field of vision and the actual area being measured is known. An aperture is then selected so that the entire spot but as little background as possible as measured. With the dimensions of the experimental set-up, the six minute aperture corresponds to a spot of about 1 mm on the screen and was used most of the time. By increasing the high voltage on the photomultiplier, the instrument can be adjusted for maximum sensitivity and after calibration can measure intensities in the 10^{-2} Footlambert range with the six minute aperture. In this mode instrument noise is 5% of full scale with no signal applied.

3. Photographic Method

In the early days of X-ray crystallography structure determinations were often done using intensities computed from the visual evaluation of the optical density of photographic plates. Photographic techniques continued to play an important role in obtaining the intensities of points in the diffraction pattern, although today many investigators use scintillation counter devices. It was a natural consequence of photography's great success in X-ray diffraction that someone try to

develop an analogous method for LEED.

When a photographic plate is exposed to X-rays or visible light, some of the silver halide grains in the film's emulsion absorb quanta of radiation and it is believed that a small nucleus of silver is formed. This nucleus constitutes the film's latent image and upon development, grains with a silver nucleus of sufficient size are then reduced to silver while unsensitized grains remain unchanged. Each absorbed quanta of light produces one silver atom but experiments indicate that with visible light about 300 quanta must be absorbed for the entire grain to be reduced during development.[24] Thus the amount of silver depends both upon the intensity of the incident radiation and the degree to which the development process reduces grains of silver iodide with some silver atoms. Under conditions of uniform development the density of silver atoms should be proportional to the light quanta absorbed. In the development process the remaining silver halide grains are removed from the gelatin of the film so the density of silver atoms can be indirectly measured by the extent to which the amount of light transmitted by the gelatin is changed. Using the familiar definition of transmission

$$T = I/I_o$$

the optical density of the film is defined as

$$O.D. = \log 1/T.$$

By plotting optical density versus the log of exposure for a given film one obtains the characteristic curve for that film using that particular method of development. Since silver density depends upon both the original quanta absorbed and the development process, the same film can have a number of different characteristic curves depending upon development. Figure III-4 shows a typical characteristic curve. The area AB corresponds to an underexposed film and results from the fact that some of the silver halide grains which absorbed light did not have a big enough silver nucleus to be developed. The linear portion BC is the range of correct exposure while the shoulder at CD corresponds to the saturation point at which most of the silver halide has been reduced and now silver atoms are absorbing additional quanta of radiation.

Exposure is usually defined as $E = \int I dt$ for normal incidence and with constant intensity this becomes $E = It$. The reciprocity law states that the characteristic curve of a film depends only upon the product It and not upon the individual factors. If the characteristic curve of a film and the time of exposure is known, the original incident intensity from the source can be calculated from measurement of the optical density of its photograph and this is the basis of the photographic technique. The reciprocity law is generally true for X-rays but for visible light it often fails at either extreme of the factors, i.e. high intensities with short times or low intensities with long times. In this case the characteristic curve of the film would be different depending upon whether current or time were held constant

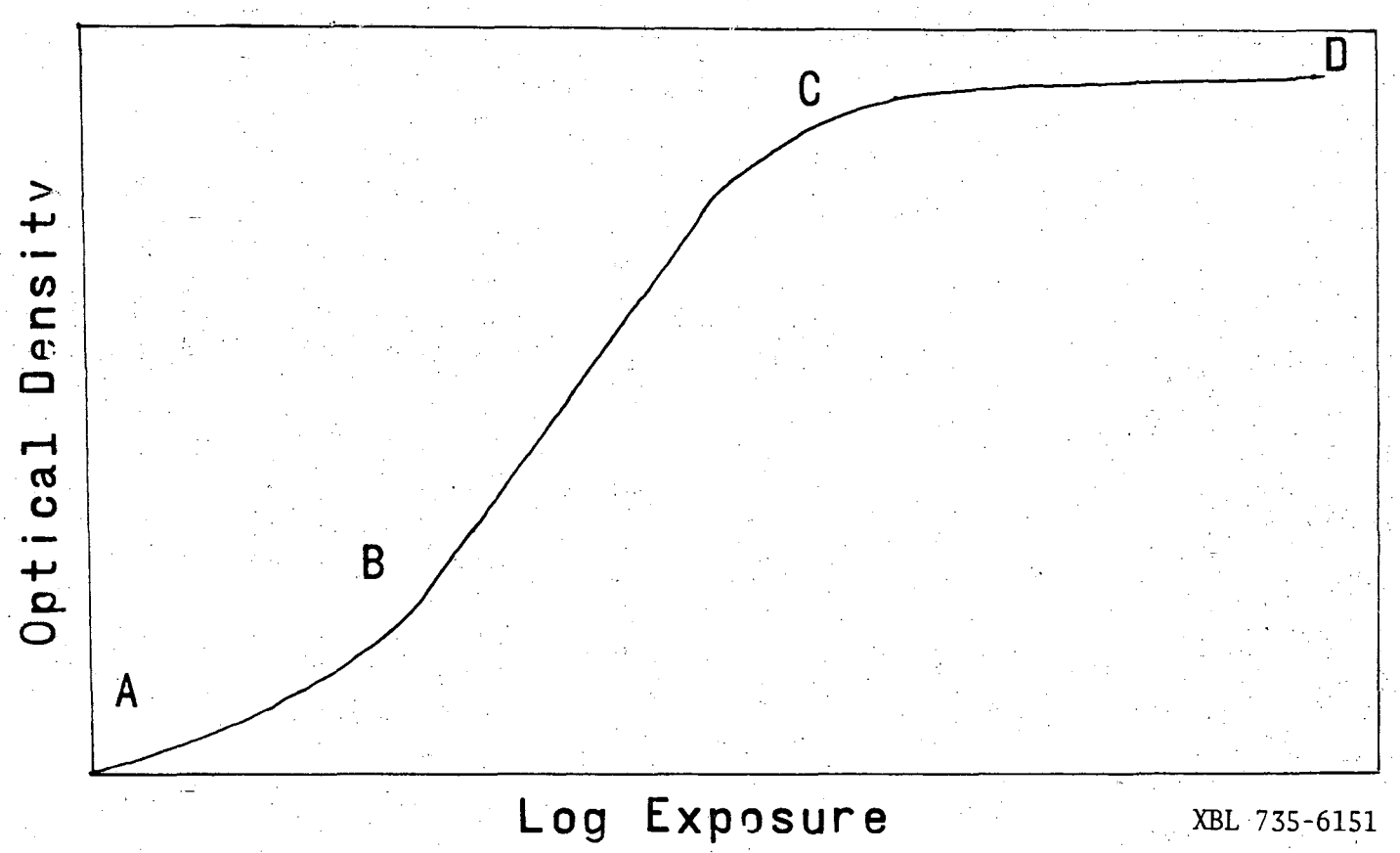

Fig. III-4. A typical characteristic curve, AB is the region of underexposure, BC is the linear portion, and CD is the overexposed region.

and its actual value.

An automatic recording microdensitometer Model MKIIIC from Joyce, Loebl & Co., Limited, England was used to measure the optical densities of the photographs. A schematic of the instrument appears in Fig. III-5. The light source at A is split into two beams. After focusing and collimation, the beams pass through the sample and reference stages. The image from the film on the sample stage is magnified and slit F defines the actual area to be measured. On the reference side a similar slit allows an equal portion of the beam to pass through the optical wedges which are plates with a continuous range of calibrated optical density. The shutter H alternates in passing sample and reference beams through to the photomultiplier tube G. If the sample and reference beams are of different intensity, a signal is fed to the amplifier k which then causes the serve motor L to move the reference optical wedge I until both beams have equal intensity. Feedback from the motor to the amplifier is provided so that the system's sensitivity can be controlled. The recorder M is physically connected to the sample stage E so that its x axis is proportional to the sample's position. Signal from the amplifier k controls the pen so optical density versus position is plotted. An assortment of optical wedges is available which determine the range of optical density that can be measured and the resolution. The wedge used in these experiments had a range of 2.6 units O.D. with a change of .13 O.D. 1 cm. The aperatures were continuously variable from 0 to 3 mm in width and 0 to 25 mm in height, and could be adjusted in .02 mm increments. Since the physical aperature must be

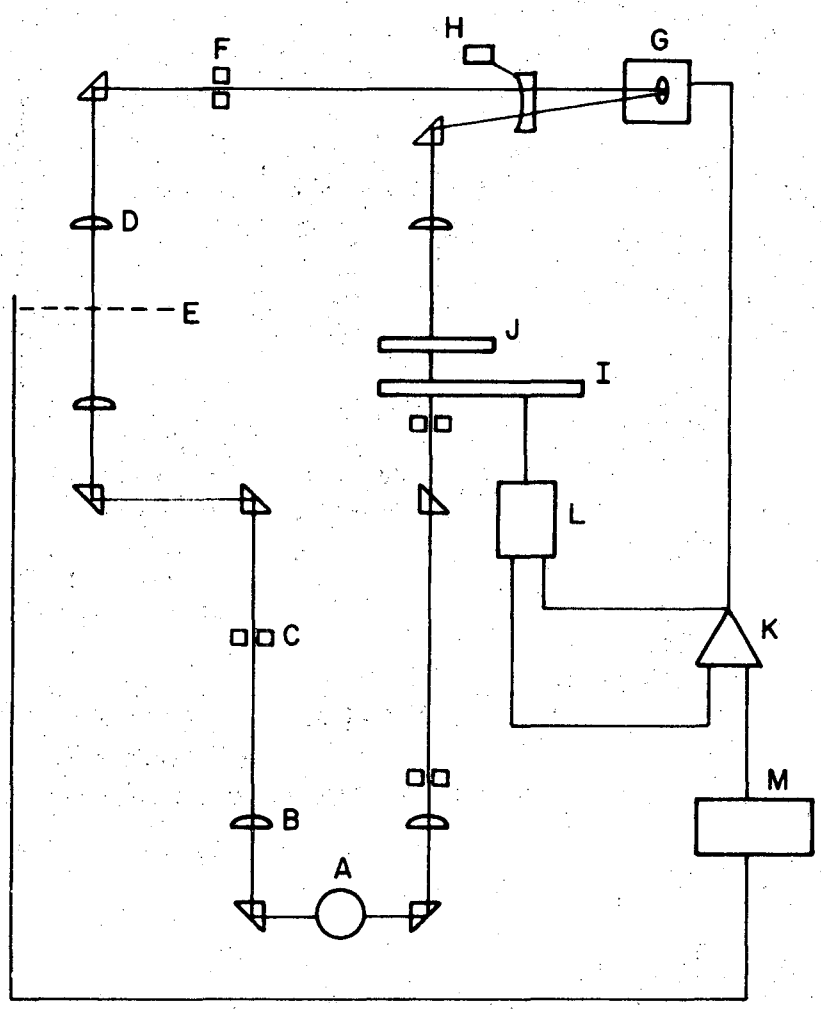

A = Lamp
B+C = Beam Focusing System
D = Magnification Lens
E = Sample Stage
F = Slit
G = Photomultiplier
H = Shutter
I = Optical Wedge to get density of sample
J = Optical Wedge to adjust baseline
K = Amplifier
L = Motor to move optical wedge I
M = Recorder

XBL 7211-7309

Fig. III-5. Schematic of the scanning microdensitometer.

divided by the overall magnification of the system to get the effective aperture size, extremely small portions of the sample could be scanned.

The procedure used in performing intensity measurements will now be described. Since the average brightness of a diffraction spot was from 10^{-1} to 10^{-3} Footlamberts for the surfaces studied with this LEED apparatus, a fast film was selected to obtain reasonable exposure times. The validity of the reciprocity law under these conditions was tested in the following way. A bright diffraction pattern was obtained and the intensity of one spot was measured with the spot photometer. A number of photographs at various exposure times were then taken. It was assumed that the intensities of the diffraction beams did not change with time. This is reasonable for a clean surface provided that the change in surface coverage while the pictures were taken was small. Since there is approximately two and a half hours of working time at 2×10^{-10} Torr and the calibration pictures took about 45 minutes, this is reasonable. Next photos of diffraction spots of different intensities were taken holding the time constant after the intensities had been measured by the spot photometer. By determining the optical densities of the spots on these photographs, two characteristic curves, one at constant intensity and the other at constant time, could be plotted. The general shape of the curves agreed within the relevant range of exposure and so the reciprocity law was obeyed. Because film sensitivity depends upon the wavelength of the incident light, the characteristic curve of a given film must be determined with the same light source as used in the experiment.

Before each experiment, pictures were taken at constant intensity but varied times to obtain a characteristic curve. After considering the range of intensities of the diffraction pattern and the film speed, an exposure time was selected that would place the optical density of most of the photographs on the linear portion of the characteristic curve. Pictures of the pattern at different beam voltages were then taken keeping the exposure time constant. The shutter of the camera was tripped by a solenoid connected to a timer to maximize precision. A Nikon F with a fast lens mounted on an extension bellows was used and because of the low intensities the F-stop was usually set at 1.2. The beam voltage ± .1 v, the emission current ± .1 microamp, and the time ± .2 sec were recorded for each photo.

To standardize developing as much as possible a tank capable of containing four reels of 35 mm film at a time was used. All of the tanks used in the process were placed in a water bath maintained at 20°C and every attempt was made to reproduce development times and agitation techniques as much as possible. Futhermore, photographs for a characteristic curve were included with every development batch to eliminate the effects of unavoidable variance in the process.

The height of the aperture of the microdensitometer was adjusted to the average spot diameter with a minimum of background included. Although the grain size of a fast film is rather significant, the aperture was large enough to integrate over the density variation of the grain distribution. The film was aligned on the sample stage visually so that the light beam was focused on the center of the spot.

The alignment was checked with the fine adjustment controls by centering for maximum optical density. The sample stage was then displaced and the scan begun from one side of the spot through to the other so that the background intensity was measured. Integration in the vertical direction of the photograph was accomplished by the photomultiplier tube so a plot of optical density versus x distance was obtained. A baseline was established to eliminate the background contribution to the spot intensity. A uniform distribution of the phosphor on the screen is assumed but even if this is not entirely the case, part of the resultant error will be eliminated with consideration of the background. An integrated spot optical density was obtained by determining the area under the curve of O.D. vs x with a planimeter. This is a device which mechanically measures the area of a figure by tracing out its circumference. Inserting an integrating circuit into the densitometer is an alternative method. The integrated densities of the calibration photographs are used to plot a characteristic curve like the one in Fig. III-6. Normalized intensities are calculated with the optical densities of the experimental pictures by finding exposure from the curve, dividing by the time to get I and then dividing by the incident beam intensity I_o from the normalization curve.

The photographic technique contains a number of variables, this makes it very flexible but at the same time is a serious disadvantage when trying to obtain high precision. A systematic treatment of these variables and their relative importance in intensity determinations follows.

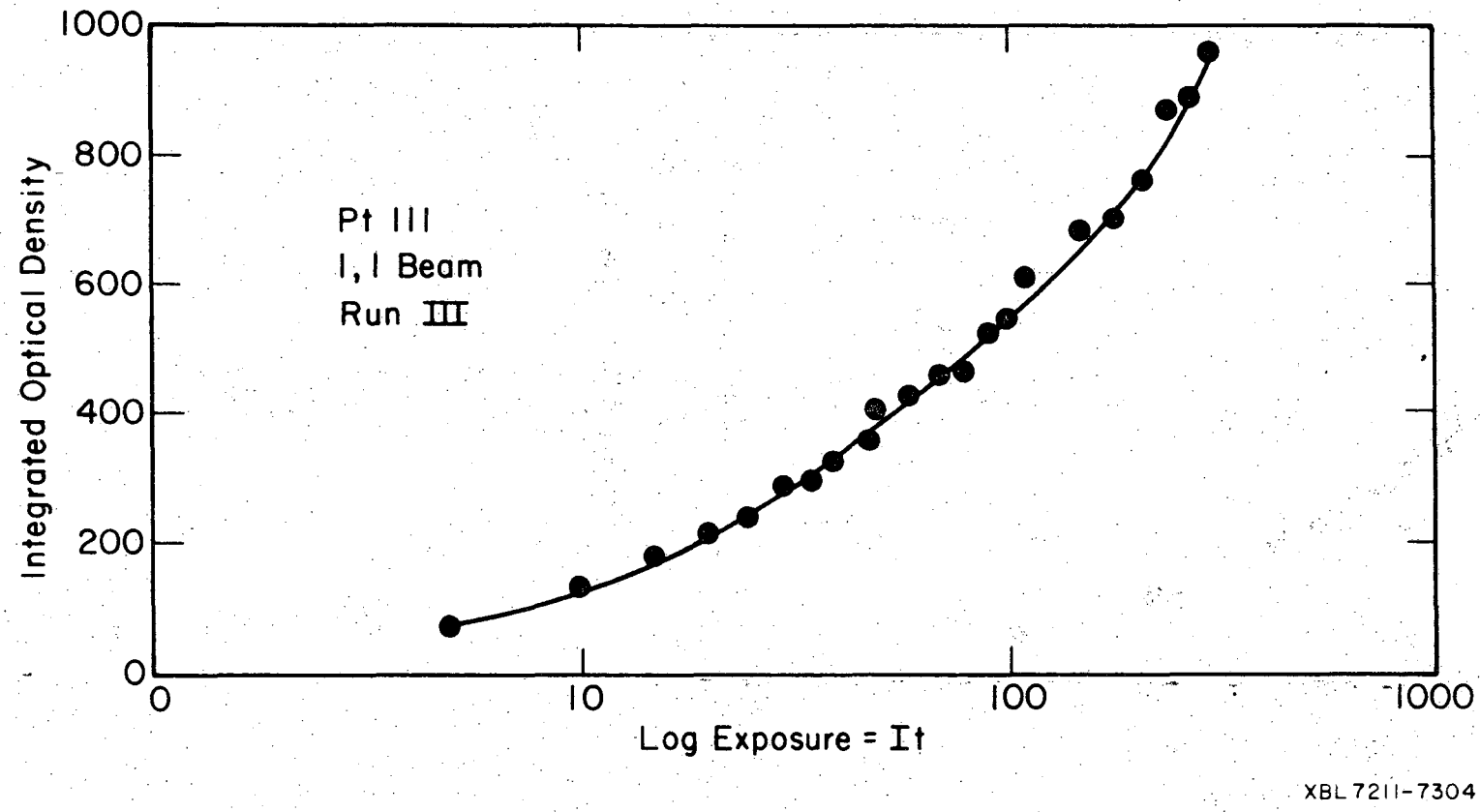

Fig. III-6. Characteristic curve for Tri-X in HC 110 using the (11) beam of Pt(111) at 60V.

It was previously mentioned that a film sensitivity varied with the wavelength of the incident light. In general, film response is peaked at about 4500 Å or in the blue region, even panchromatic films which have been treated to widen the sensitivity range behave in this way. However, the human eye is most sensitive to yellow-green light from about 5400 to 5700 Å. So a phosphor which photographed well might be almost impossible to see. Since a number of phosphors with different radiant energy distributions are available, one would want to pick a blue phosphor to achieve maximum film sensitivity and yet still be able to see a diffraction pattern. Table III-1[25] lists some phosphors, the color of their fluorescence, their relative luminance, and relative film sensitivity. Luminance is the measurement of the intensity of a light source with an instrument which has been calibrated to the spectral response curve of the eye.

Table III-1

Type	Fluorescence	Relative Luminance	Relative Film Sensitivity
P1	Yellowish Green	45	35
P4	White	50	75
P7	Blue-White	45	95
P11	Blue	25	100
P31	Green	100	75

P31 is the phosphor usually used in oscilloscopes. Unfortunately it has a vapor pressure which is too large for ultra high vacuum work, P7 might be a good choice, but it has a decay time of over a minute which would make quick scans of the diffraction pattern over a range of beam voltage impossible. P4 is the phosphor normally used in Varian LEED display systems having replaced P1, but P11 was chosen for this research to maximize film sensitivity, even though it is one half as bright visually.

Since the light intensity of diffraction patterns viewed in the LEED apparatus is quite low, a fast film is desirable to shorten exposure time. However, fast films are usually accompanied by large grain size and since the grain size of the film is directly related to the intensity resolution of the method, one would like to keep grain size at a minimum. As was mentioned earlier, grain refers to the size of the silver halide particle containing the light sensitized silver nucleus that is then reduced to silver in the development process. If the area of the film exposed to the intensity of a diffraction spot contains only 10 grains, it is obviously much less sensitive to small intensity variations than a film which had a 1000 grains in the same area. Developers are available which will boost the effective speed of a fine-grained film but again the price is paid by an increase in grain size and a decrease in resolution. So, as is usually the case in life, a compromise must be made between film speed and grain size to make the optimum selection. A variety of films and developers were tried and Kodak Panchromatic Tri-X and

Kodak 5479 were found the most suitable. Table III-2 lists some of the films, the developer, the time required for developing at 20°C, the film speed with that developer in ASA units, and the relative grain size where Tri-X in DK-50 was considered average.

Table III-2

Film	Developer	Development Time	Film Speed (ASA)	Relative Grain
Tri-X	Accufine	5 1/4 min.	1200	largest grain
Tri-X	HC-110 Dilution A 1:3 ratio stock developer to water	4 1/4 min.	400	smallest grain
Tri-X	DK-50	6 min.	400	average
Tri-X	D-76	9 min.	400	average
5479	D-76	10 min.	800	slightly larger than average

Kodak 5479 is a film designed to record oscilloscope displays and proved to be twice as sensitive to light emitted by the P11 phosphor as Tri-X. The developers used are all commercially available and except for Accufine are produced by Kodak. Fresh developer solution was used for each set of film to be developed. After developing, the film was rinsed in Kodak Indicator Stop Bath for 30 seconds, then placed in Kodak Fixing Bath F-5 for six minutes. The film was washed in

running water for 17 minutes, dipped in Kodak Photoflo solution to minimize drying marks, and then forced air dried for 20 minutes. A Gra-Lab timer with a phosphor face readable to one second was used for timing purposes. The film was agitated manually in development, stop, and fixer baths continuously for the first minute and then for five seconds at minute intervals. Because the exposure time was not extremely critical in these experiments, maximum resolution was desirable. Tri-X in HC-110 was selected since its grain was significantly smaller than the other combinations. For the surfaces studied with this apparatus, an exposure time of 40 seconds was used to give a range of optical densities on the linear portion of the characteristic curve.

Once the phosphor, film, developer, and exposure times are chosen one must consider the control of the variables in the experiment itself and in the subsequent steps necessary to the calculation of normalized relative intensities.

Treatment of the variation of the incident beam current has already been described. The crystal temperature greatly affects the scattered intensities because of the Debye-Waller factor. All experiments were performed at room temperature to eliminate temperature as a variable. Both the potential on the fluorescent screen and that on the suppressor grid will affect the intensity of light for a given beam intensity. These were adjusted to a constant setting before the calibration photos were taken for each experiment. Since relative intensities are calculated from the resultant characteristic curve, any variation is taken into account. Standardization of the exposure time by a solenoid-tripped

shutter has already been mentioned. Although quality control in the film industry is quite high, every batch of film made has slightly different response characteristics due to the variation in the quality of the ingredients used. Cassettes were hand loaded from a 900 foot reel of Tri-X film so that the film used was completely uniform. Since development greatly affects optical density, this is an extremely important variable and the inclusion of a characteristic curve with each development batch is essential.

The scanning procedure with the microdensitometer is also designed to maintain a consistent treatment of the film. The instrument is calibrated each time after selection of the slit size, pen response, and optical density scale. Using the same method to center the diffraction spots should prevent low values due to missing most of the spot in a scan. In integrating the optical densities of the scans a base line for the calibration pictures is set at the optical density level of an unexposed part of the film. The baseline for the LEED experimental negatives is set at the background level around the spot.

It is clear from the discussion that the photographic method is indirect with a number of steps between the actual scattered electron beam intensity and the final normalized relative intensity computed from the data. By following the described procedure to control the variables inherent in these steps it is hoped that accurate measurements of relative intensities can be made. The advantages of the method are a permanent record of the primary data and the short experimental times required to measure the intensities of an entire diffraction

pattern. In studying the complicated diffraction patterns of a surface structure formed by an overlayer these advantages are important enough to more than outweigh the drawbacks.

E. Intensity Data

1. Clean Metal Surfaces

The experiments were performed with platinum single crystals of (111) and (100) orientation mounted back to back on the sample holder so that both surfaces could be studied without opening the system to atmosphere to change samples. A slight adjustment of the manipulator brought the surface of the desired crystal to the center of curvature.

Platinum is a face-centered cubic crystal, the (111) face has hexagonal symmetry with the surface unit cell the same as the bulk. Figure III-7 shows a picture of the diffraction pattern from a clean platinum (111) surface at 60 volts. The top half of Figure III-8 illustrates the unit vectors and spot labels chosen in this work to agree with Jona's terminology.[26] θ, the angle of incidence and ϕ, the azimuthal angle are defined in the diagram in Fig. III-9. Intensities of the (00) beam were measured by the spot telephotometer at five volt intervals from 50 to 150 volts. At normal incidence, the specular beam is reflected back into the gun and is not observable so the measurements were made with $\theta = 7°$ and $\phi = 0°$. These results, after normalization by the incident beam current, were compared with relative intensities of the (00) beam obtained by the photographic technique under the same experimental conditions. The I vs V curves for the two methods are

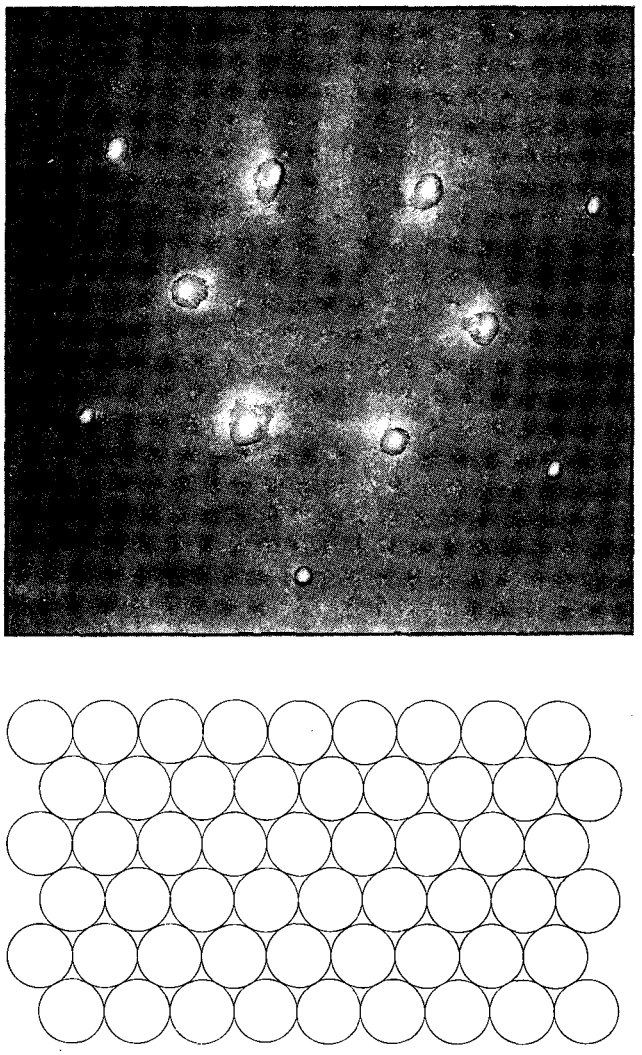

XBB 7110-5214

Fig. III-7. Picture of Pt(111) diffraction pattern with schematic of atomic positions showing hexagonal symmetry.

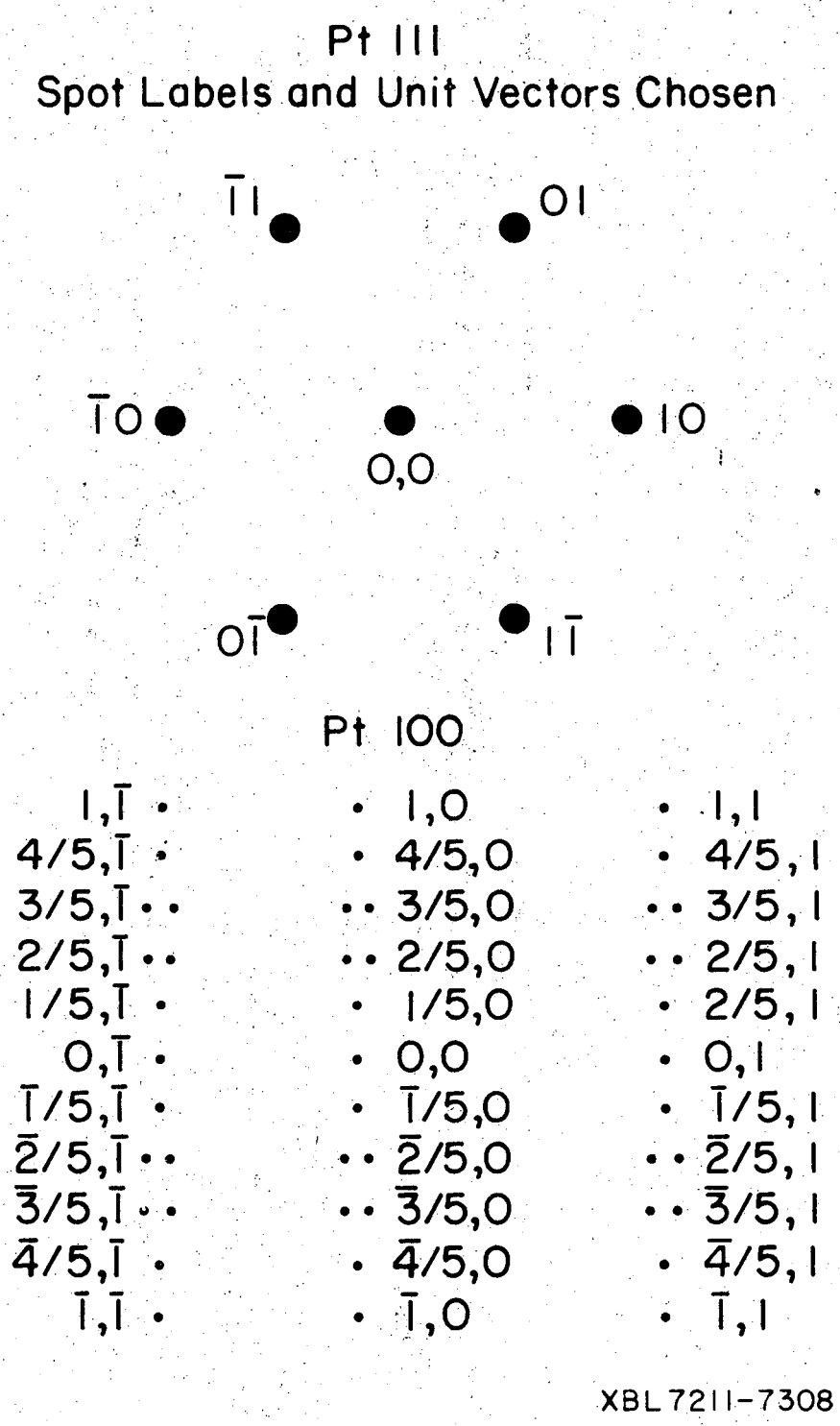

Fig. III-8. Diagram of spot labels for diffraction patterns from Pt(111) and Pt(100).

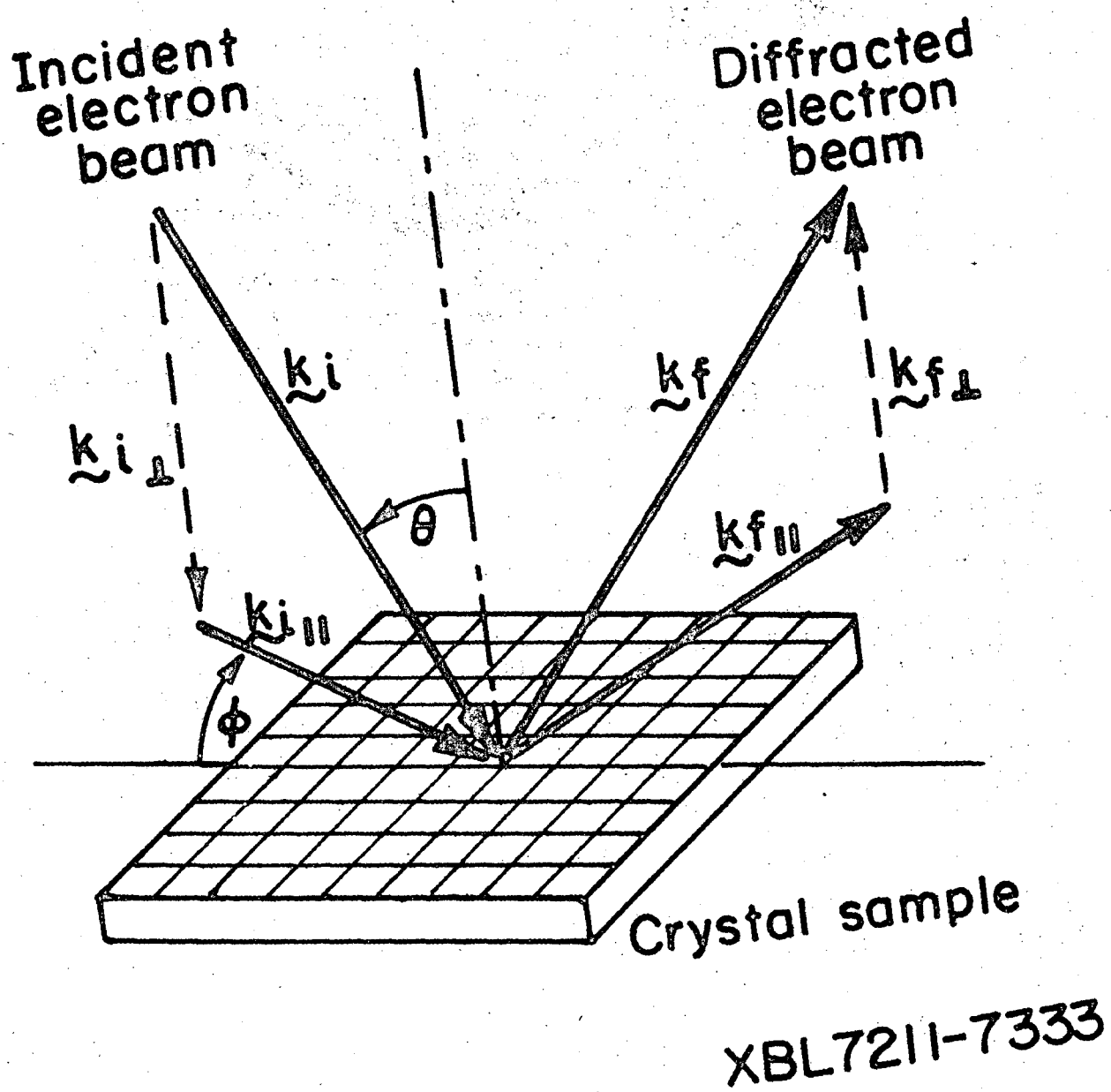

XBL7211-7333

Fig. III-9. Diagram defining θ as the angle of incidence and ϕ as the angle of rotation of a principle azimuth.

plotted in Fig. III-10. The intensities of the two methods are normalized to each other at the peak at 50 volts. Each point plotted is the average of three trials and the agreement between the two methods is quite good. At normal incidence, the crystal's symmetry causes a degeneracy in the diffraction pattern so that the (01), $(1\bar{1})$, and $(\bar{1}0)$ beams are equal to each other and the $(\bar{1}1)$, $(0\bar{1})$, and (10) beams are also degenerate. Therefore, in the range of 50 to 150 volts only two nonspecular beams need be measured. The normalized intensities of the (10) and $(1\bar{1})$ beams at normal incidence were measured by using the photographic approach and appear in Figs. III-11 and III-12. Again the points plotted are averages of three trials with the maximum deviation 10%.

The surface reconstruction of the (100) face of platinum has been studied for a number of years and indeed during that time has rarely been free from controversy. The clean surface of Pt(100) has been found to rearrange to give a unit cell that is five times the length of the bulk unit cell along one vector and equal to the bulk cell along the other. Figure III-13 contains a photograph of the (5×1) diffraction pattern at 63 volts formed by two ordered domains rotated 90° from each other. The photographic technique greatly simplifies the measurement of the intensities of the nonspecular beams in a complicated pattern such as this one. The lower part of Fig. III-8 illustrates the spot labels chosen for the (5×1) diffraction pattern resulting from one domain. Note that the unit vectors and spot labels chosen here are different from the ones chosen by Jona for Al(100) in

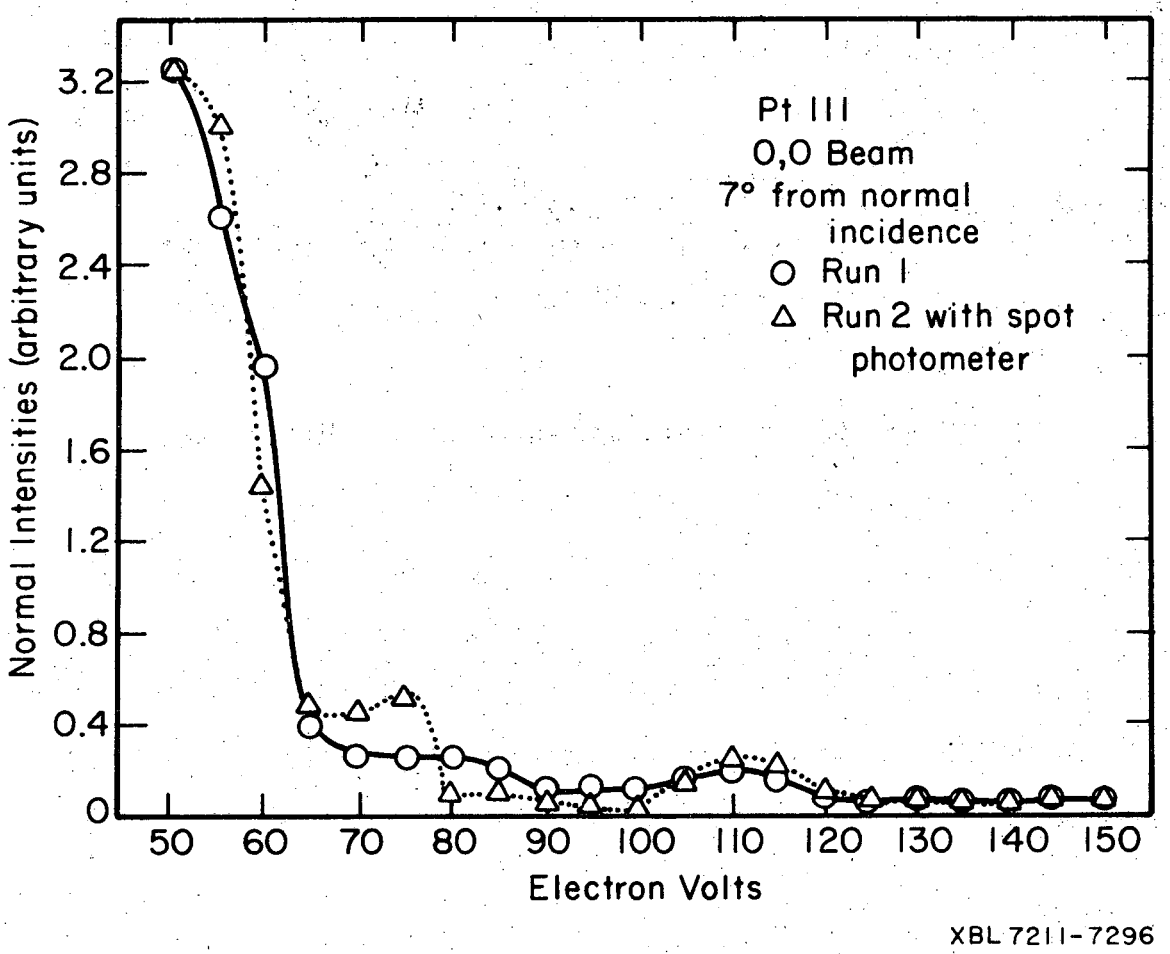

Fig. III-10. I. vs V. curves for (00) beam of Pt(111) with $\theta=7°$ and $\phi=0°$.

0 0 0 0 3 9 0 0 9 2 3

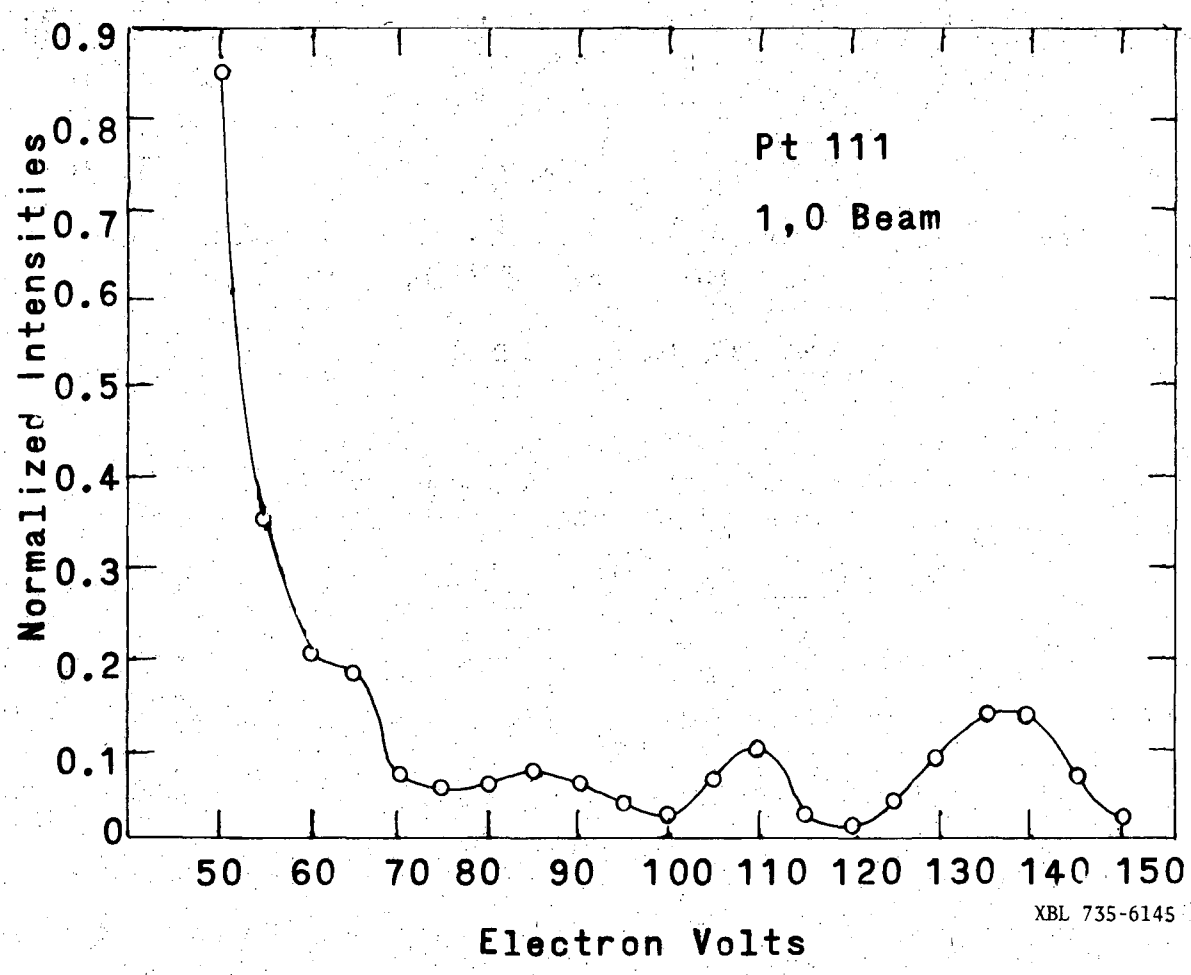

Fig. III-11. I. vs V. curve for (10) beam of Pt(111) with $\theta=\phi=0°$.

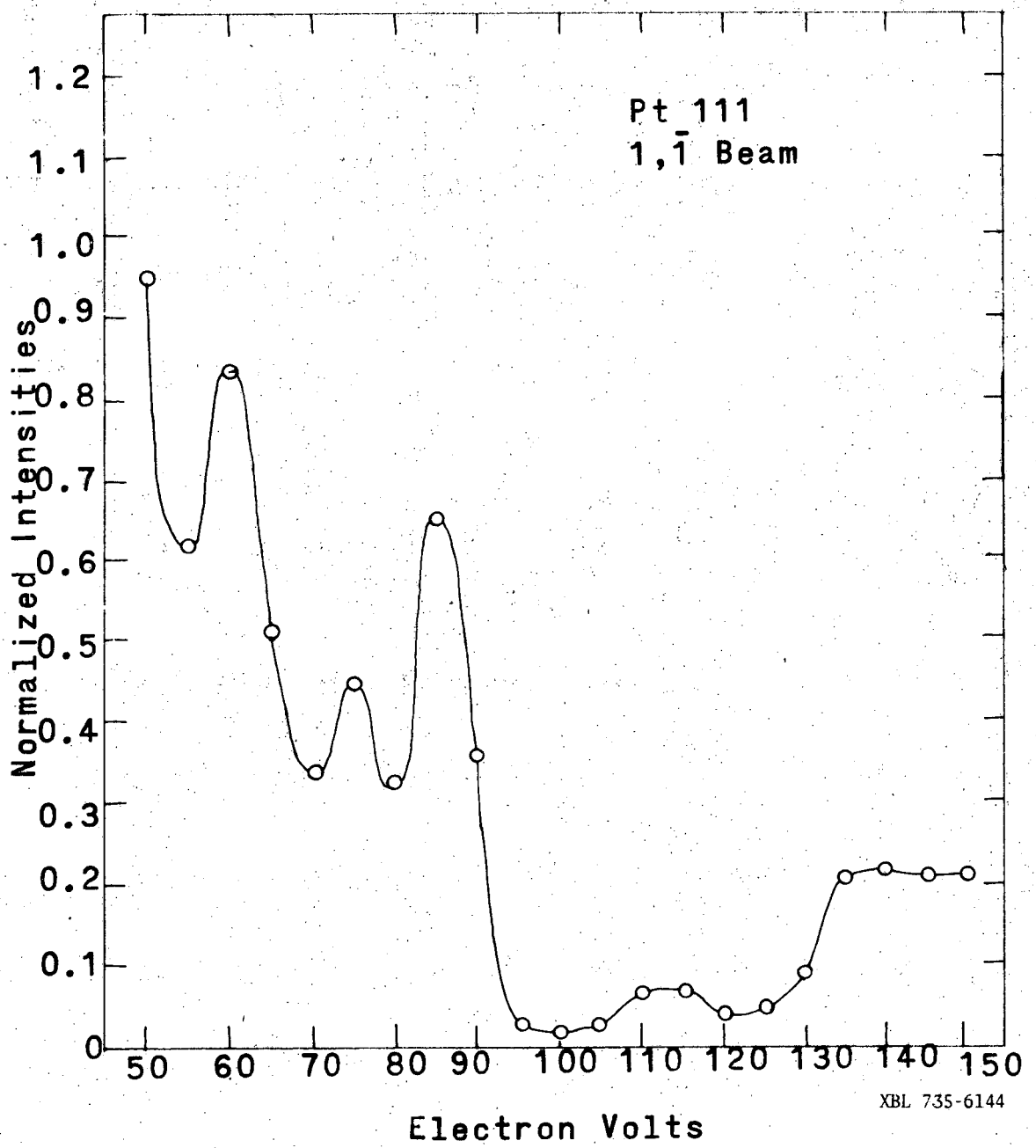

Fig. III-12. I. vs V. curve for (1$\bar{1}$) beam of Pt(111) with $\theta=\phi=0°$.

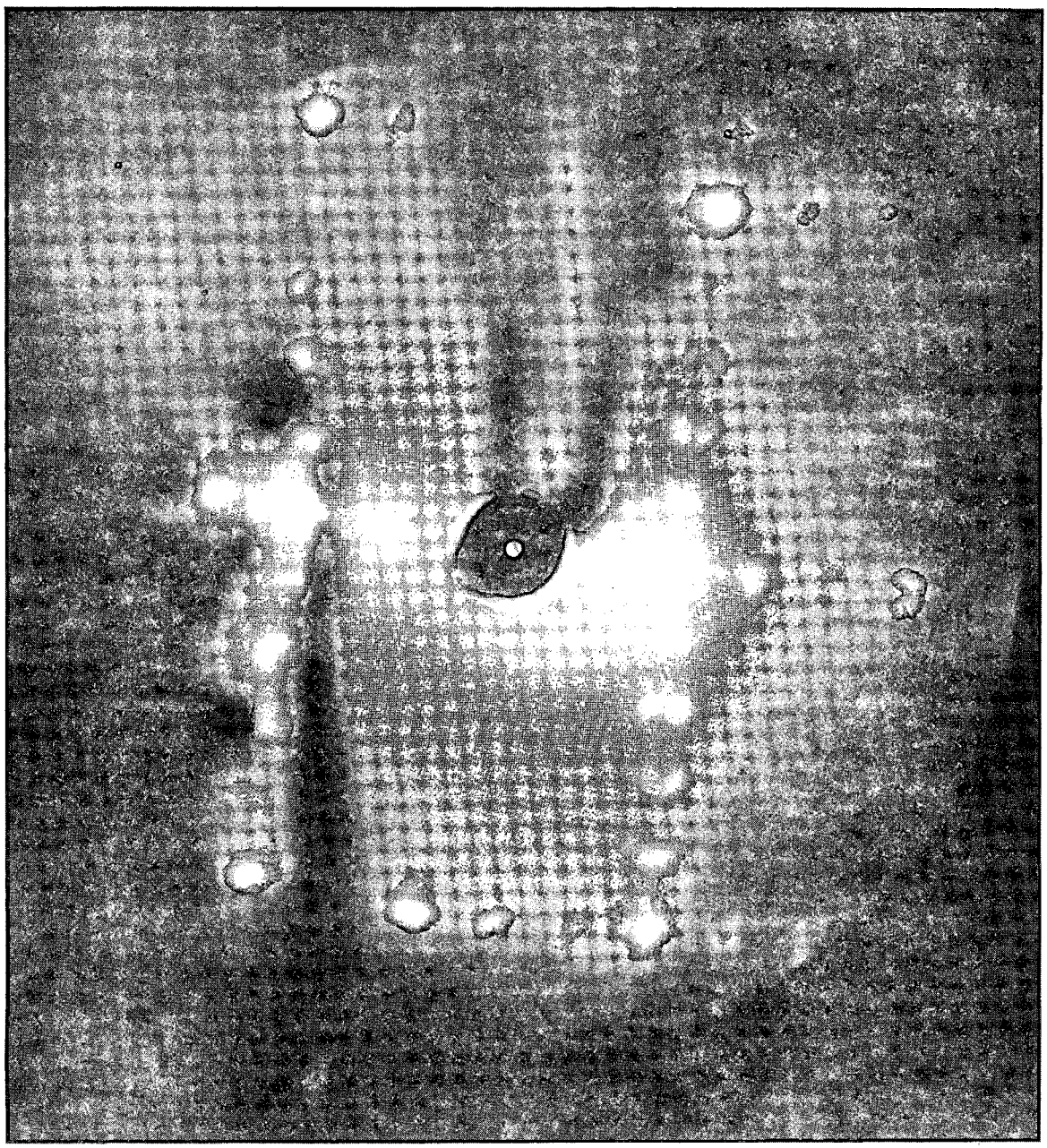

XBB 708-3757

Fig. III-13. Photograph of (5×1) diffraction pattern from Pt(100) at 63 volts.

the paper cited although Jona's definition for determination of the azimuthal angle ϕ will still be used. If a vertical and horizontal line are drawn through the (00) spot at normal incidence the crystal's symmetry causes diffraction beams on opposite sides of the line to be degenerate. In this case eleven beams must be measured to characterize the entire pattern. No attempt was made to correct for the contribution from the other domain to beams like the (10), (01), $(\bar{1}0)$, $(0\bar{1})$, (11) etc. A close examination of the photograph in Fig. III-13 reveals that many of the fractional order beams are actually doublets. One would like to measure the intensity of these doublets without including the background between them. The light intensity of one segment of the doublet is often so low that this would be very difficult with the spot photometer. However with the photographic technique, the scanning microdensitometer gives one a record not only of the intensity of each part of the doublet but the diffuse intensity spreading out into the background between them as well.

I. vs V. curves from 50 to 150 volts measured at 5 volt intervals are shown in Figs. III-14 and III-15. All points are averages of three trials with a maximum deviation of 15%. The (00) beam was taken at $\theta = 7°$ and $\phi = 2°$. All other beams were measured at normal incidence with $\phi = 2°$.

2. Adsorbed Overlayer

A different LEED system similiar to the one previously described was used to do the adsorbed overlayer experiments. Because the intensities of the observed diffraction beams were very low in this

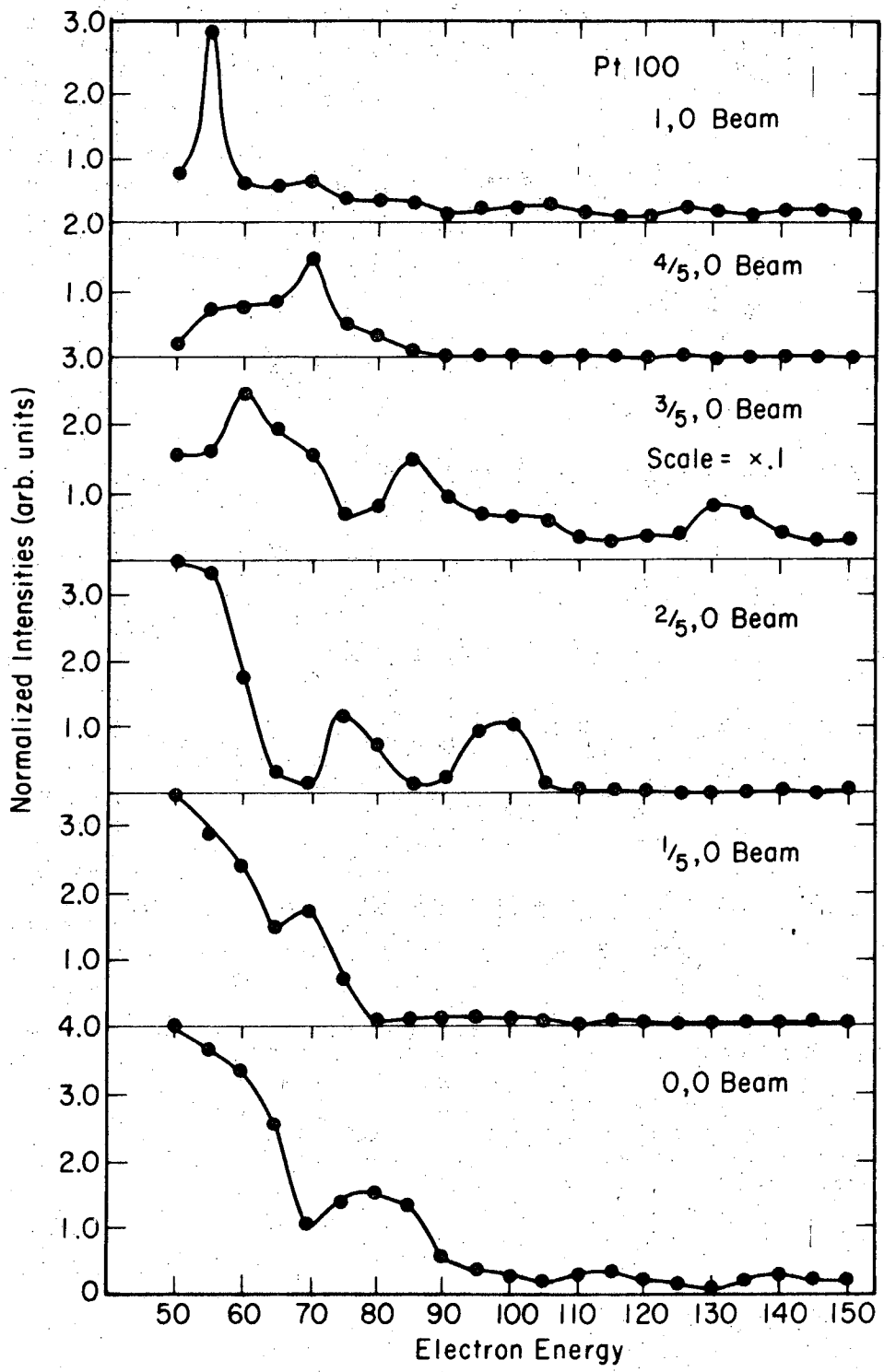

Fig. III-14. I. vs V. curves for (5×1) of Pt(100) with θ=0° (except for (00) beam) and ϕ=2°.

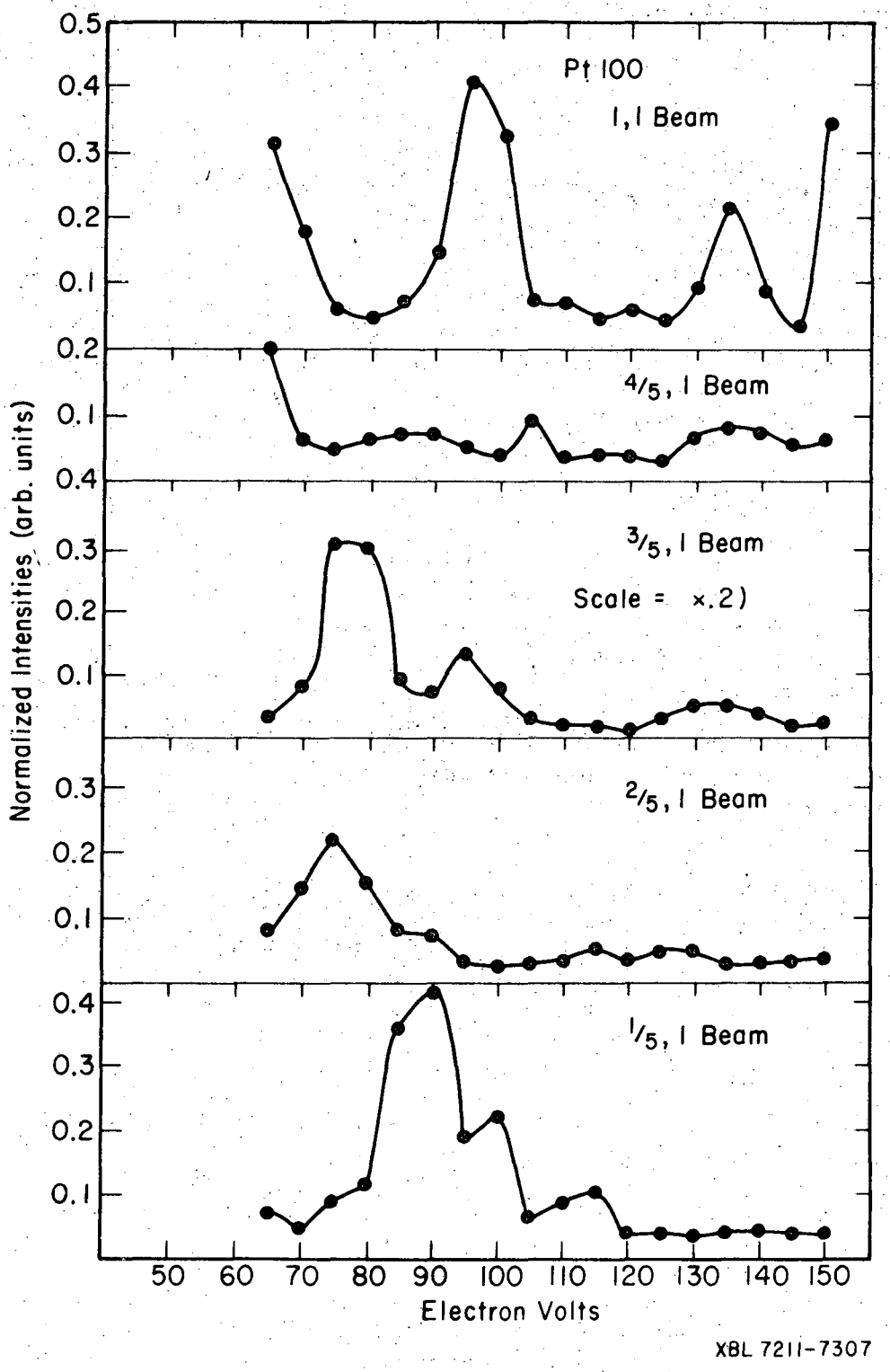

Fig. III-15. I. vs V. curves for (5×1) of Pt(100) with $\theta=0°$ and $\phi=2°$.

system, the photographic technique with maximum film speed was used to perform the measurements. Tri-X was developed in Edwal's FG7 for six minutes at 23°C to give it a film speed of approximately 3000 ASA.

Single crystals of Pt(100) and Pt(111) were mounted back to back, however it is questionable whether or not the crystals were exactly at the center of curvature of the screen. The pressure of the system before the experiment was 3×10^{-9} Torr and propylene was admitted to the system through a capillary aimed at the crystal. Although the pressure in the immediate vicinity of the crystal could not be measured, pressure at the ionization gauge during the adsorption was 6×10^{-9} Torr. After 15 minutes with a continuing flux of propylene the Pt(111) surface was observed and a (2×2) diffraction pattern was found. After 30 minutes photographs of the diffraction pattern were taken. Some of the beams and their labels for this pattern are illustrated in Fig. III-16 for $\theta = 0$ and $\phi = 0$. However, because of the hexagonal symmetry this same pattern could result from a (2×1) structure with three domains rotated 60° from each other. To distinguish between these two models the intensities must be measured. One would expect that the degeneracy observed in the diffraction pattern from the clean surface at normal incidence would be preserved by the (2×2) structure but not by several domains of a (2×1) structure. The intensities of all the beams shown in Fig. III-16 were measured and the normalized, relative I. vs V. curves are shown in Figs. III-17 to III-20. Each figure plots the three beams that would be expected to be degenerate for a (2×2) structure. Not all the beams could be continuously observed

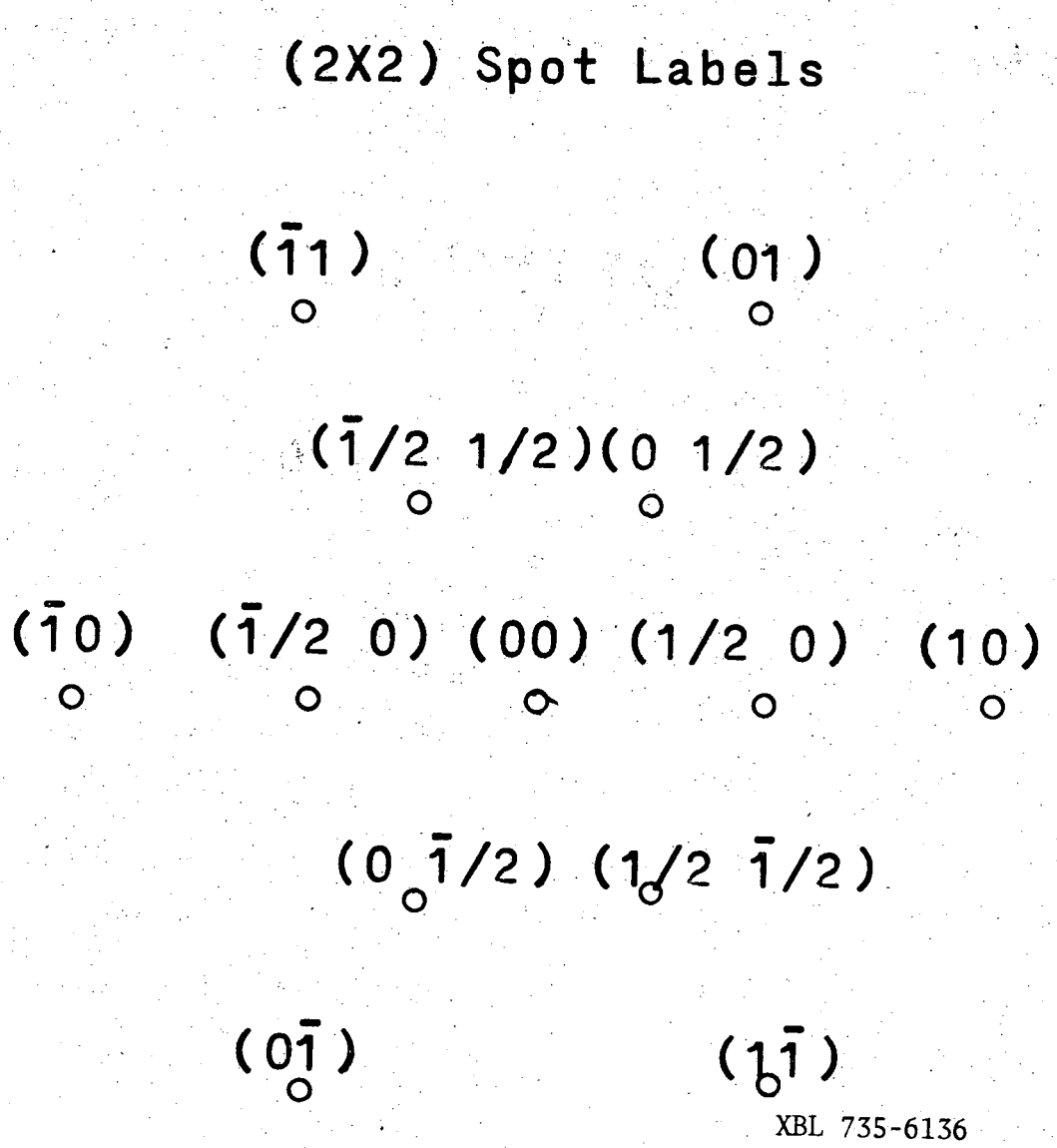

Fig. III-16. Spot labels for (2×2) diffraction pattern formed by propylene on Pt(111).

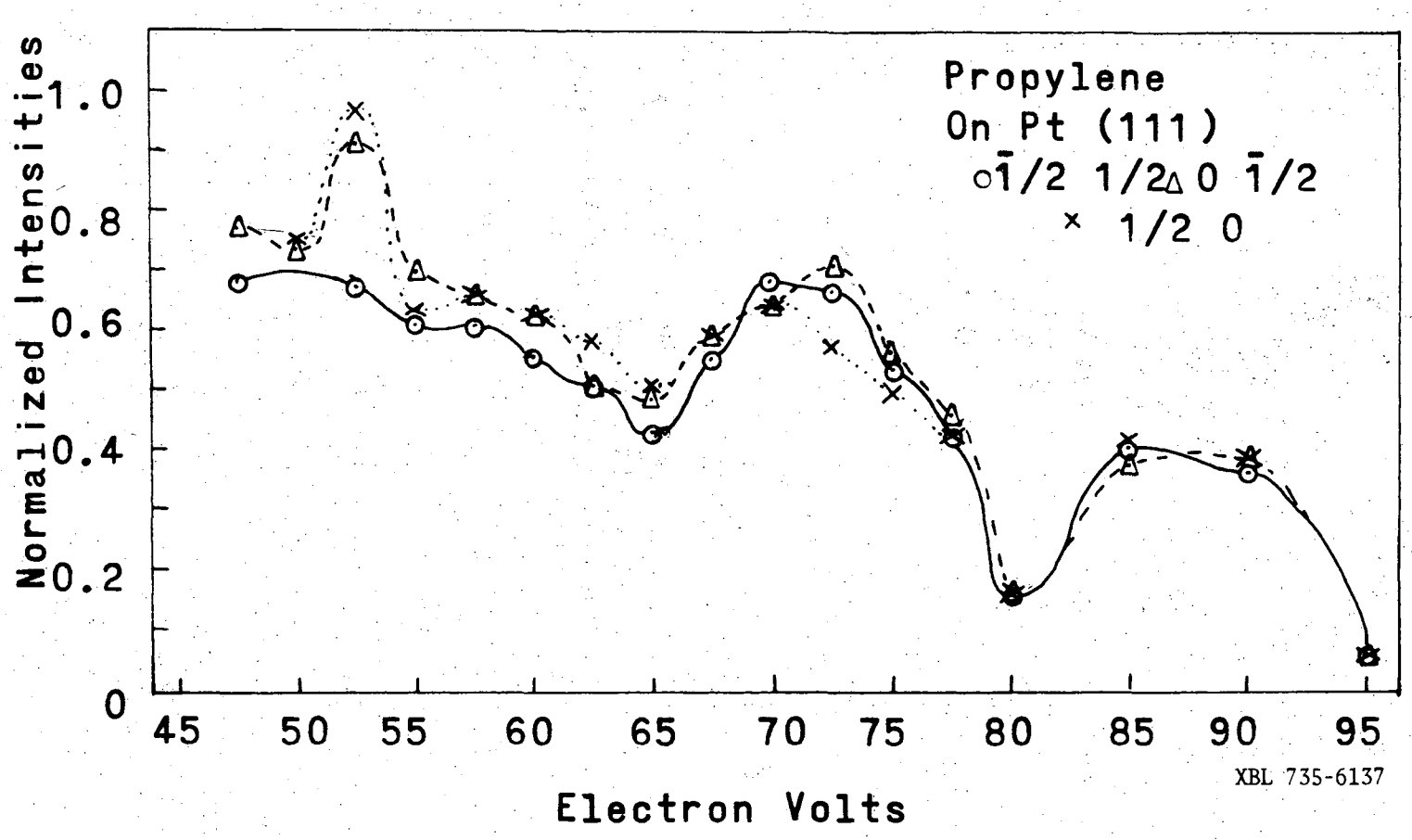

Fig. III-17. I. vs V. curves for ($\bar{1}$/2 1/2), (0 $\bar{1}$/2), (1/2 0) beams from propylene on Pt(111) with $\theta=\phi=0°$.

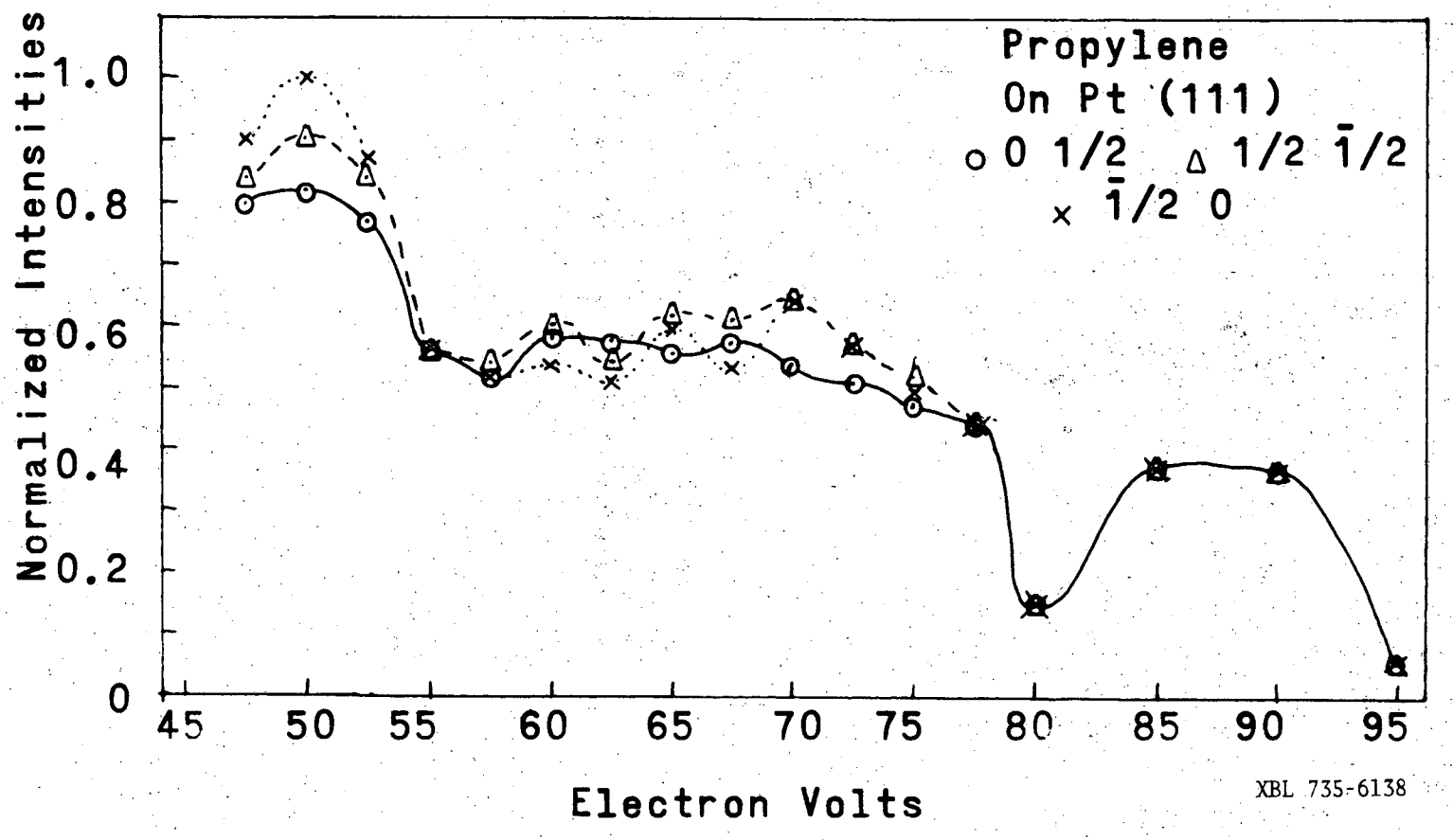

Fig. III-18. I. vs V. curves for (0 1/2), (1/2 $\bar{1}$/2), ($\bar{1}$/2 0) beams from propylene on Pt(111) with $\theta=\phi=0°$.

0 0 0 0 5 9 9 0 7 2 8

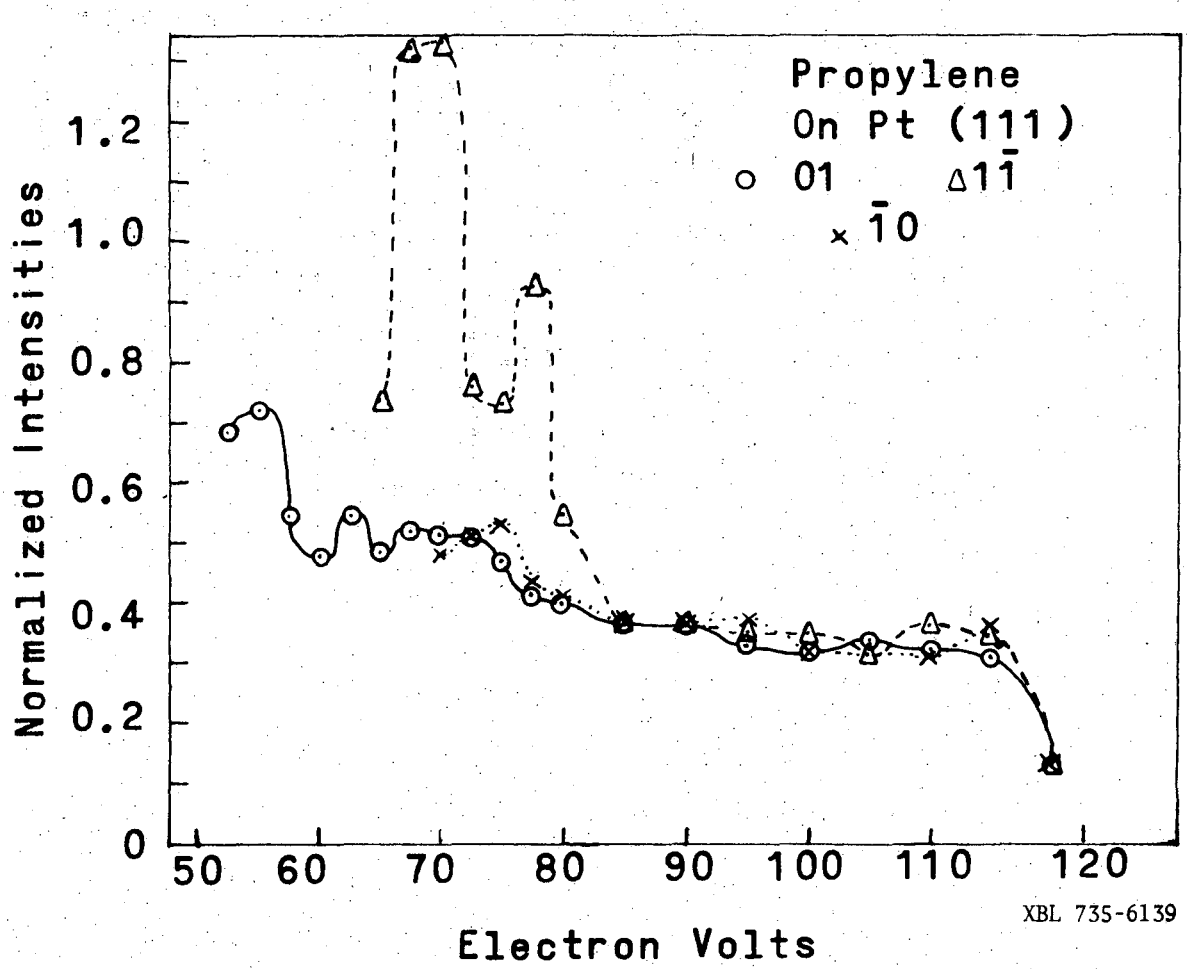

Fig. III-19. I. vs V. curves for (01), (1$\bar{1}$), ($\bar{1}$0) beams from propylene on Pt(111) with $\theta=\phi=0°$.

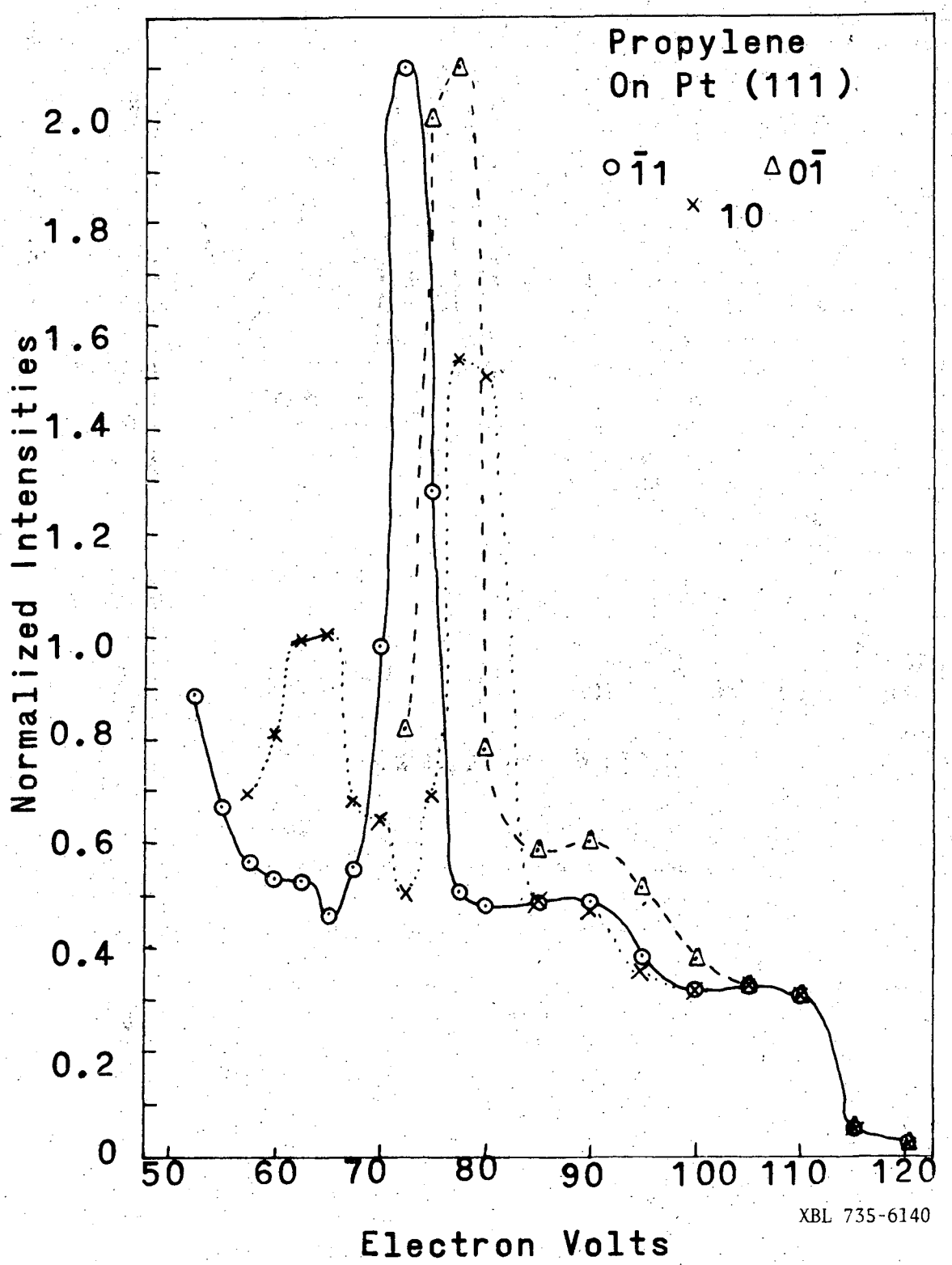

Fig. III-20. I. vs V. curves for ($\bar{1}1$), ($0\bar{1}$), (10) beams from propylene on Pt(111) with $\theta=\phi=0°$.

throughout the entire voltage range because of the experimental geometry. Because of the orientation of the crystal, the angle of incidence may be one or two degrees so failure to observe complete degeneracy would not necessarily rule out a (2×2) structure. Although there are some differences in peak heights, the shape and position of the peaks agree very well for the most part and seem to justify labeling the structure a (2×2).

IV. DISCUSSION

It has been made clear that a definitive analysis of the structure of a clean surface or a structure formed by an adsorbed layer requires both the experimental measurement of the intensities of the diffracted beams and a computational procedure that will calculate intensities from a proposed model using a suitable theory. It would appear that the multiple scattering theory for LEED intensities is sufficiently developed to give good results for simple metals where the potential is known. The main components of the scattering process have been identified, now a given I. vs V. curve depends upon the degree to which a calculated scattering amplitude approximates the actual one. Since this depends upon the phase shifts calculated from the potential of the crystal, the intensities calculated for an adsorbed layer can be varied either by changing the potential used or by changing the structure terms. While the potentials for simple metals such as aluminum and nickel have been used for quite a while and are known to work well, it is not at all certain that the same type of ion core potential in a muffin-tin approximation can be used for more complex metals like silver or platinum. The partially filled d shells of these metals may make quite a difference and some of the approximations which are made in calculating the potential may no longer be valid. To gain familiarity with the potential involved, the intensity curves of a clean surface that does not reconstruct should be measured for a strong scatterer and then compared with the curves calculated from theory.

The next step would be to see what kind of potential should be used for an adsorbed layer by depositing something with a fairly obvious potential on the surface. The experimental intensity data could be taken and then compared with the theoretical intensities to do structure analyses of simple systems. In taking the data, it would be best to look at the intensities of beams with a large wave vector component parallel to the surface such as the (10), (11), or fractional order beams since these would be more sensitive to the surface structure. One would expect the (00) beam to have little sensitivity to the slight changes in surface positions that are needed to do structure analysis.

The (111) face of platinum was chosen for such a study because of its great importance in catalysis. Preliminary calculations for several beams from Pt(111) using the computer programs previously described have been performed by Martin[27] and by Larramore.[28] Martin's procedure used four phase shifts calculated for Pt^{+3} from a modified version of Pendry's program and the perturbation approach which considered three layers of the crystal. A lattice constant of 3.92 Å was assumed. The calculation was for normal incidence with $\phi = 0°$ and at room temperature, θ_D for the surface was assumed equal to θ_D bulk or 240°K. The real part of the self energy correction used was 14.6 volts with an inelastic damping length of 5 Å.

Larramore's calculations were also for room temperature and normal incidence and assumed the same values for the lattice constant and Debye temperature as above. The calculations used five phase

shifts, a matrix inversion technique, an inner potential of 14.6 volts and an inelastic damping length of 8 Å. Figures IV-1 to IV-3 contain the I. vs V. curves for the (00), (10) and (1$\bar{1}$) beams comparing the experimental (solid lines) with Martin's results (dashed lines) and Larramore's (dotted lines). The (00) beam calculated by Martin compares quite well with the experiment especially since the calculated curves are for normal incidence. However, because of the lack of structure in the curve this is not really that meaningful. Unfortunately, even a casual glance at the other two beams tells one that very little agreement is present. Martin's curves do tend to produce the peaks observed experimentally for the (10) and (1$\bar{1}$) beams at 130-150 volts but the structure observed between 60 and 90 volts for the (1$\bar{1}$) beam is hidden within an enormous peak in either calculation. This may be resolved by adjusting the inelastic damping length which tends to make the peaks sharper and more defined but it remains to be seen. A final note of discouragement is sounded by observing the large peak at 80 to 100 volts for the (10) beam in both theoretical curves, which just does not appear in the experiment. It is hoped that these problems will be solved in the near future by manipulation of the electron self energy parameters or reevaluation of the pseudopotential used to calculate the phase shifts. Once the intensity versus voltage curves from theory match the experimental ones, the structure analysis of propene on Pt(111) will be attempted.

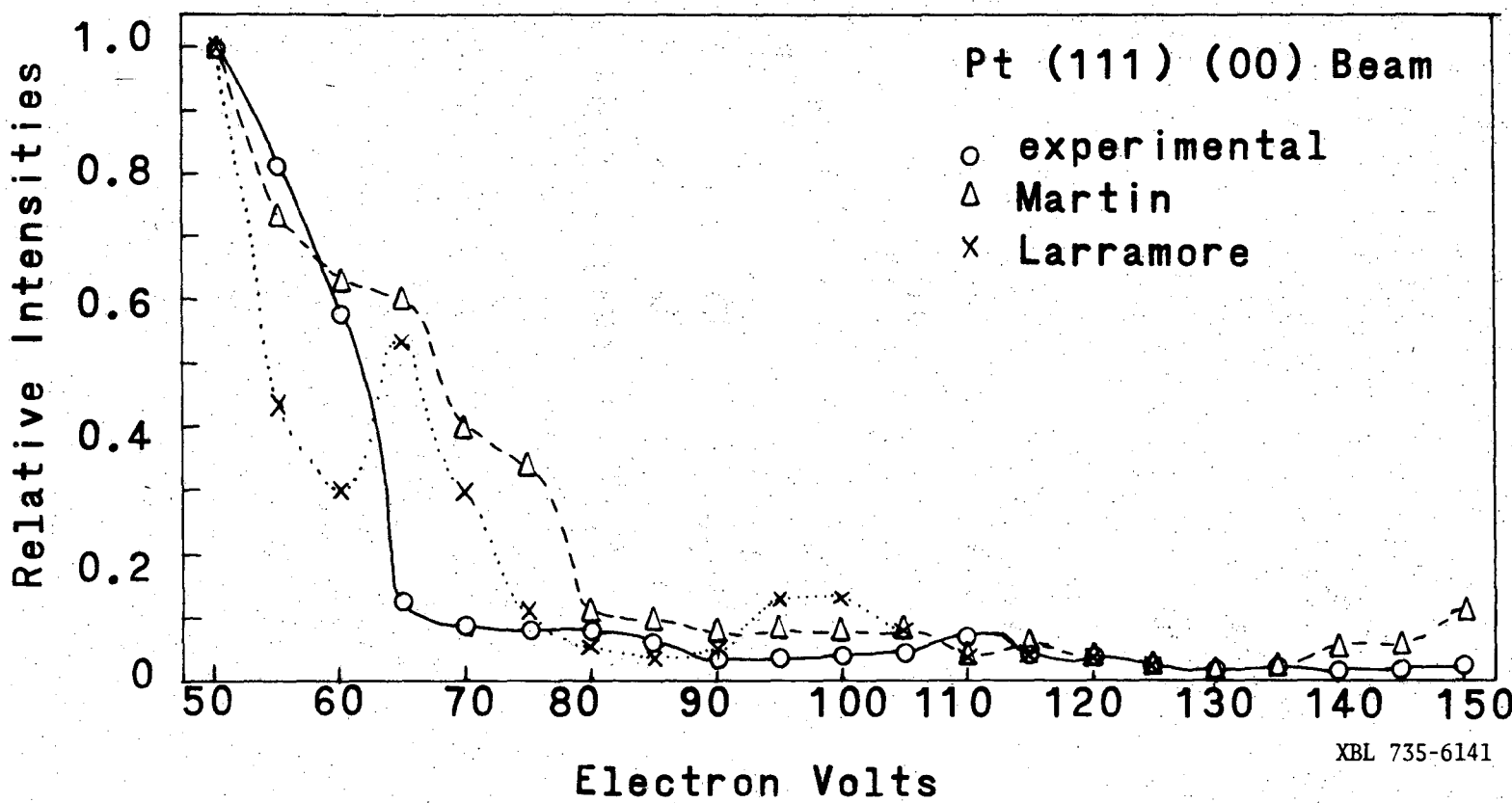

Fig. IV-1. I. vs V. curves for (00) beam of Pt(111) from experiment and multiple scattering theory; $\theta=7°$ and $\phi=0°$ in experiment, $\theta=\phi=0°$ in theory.

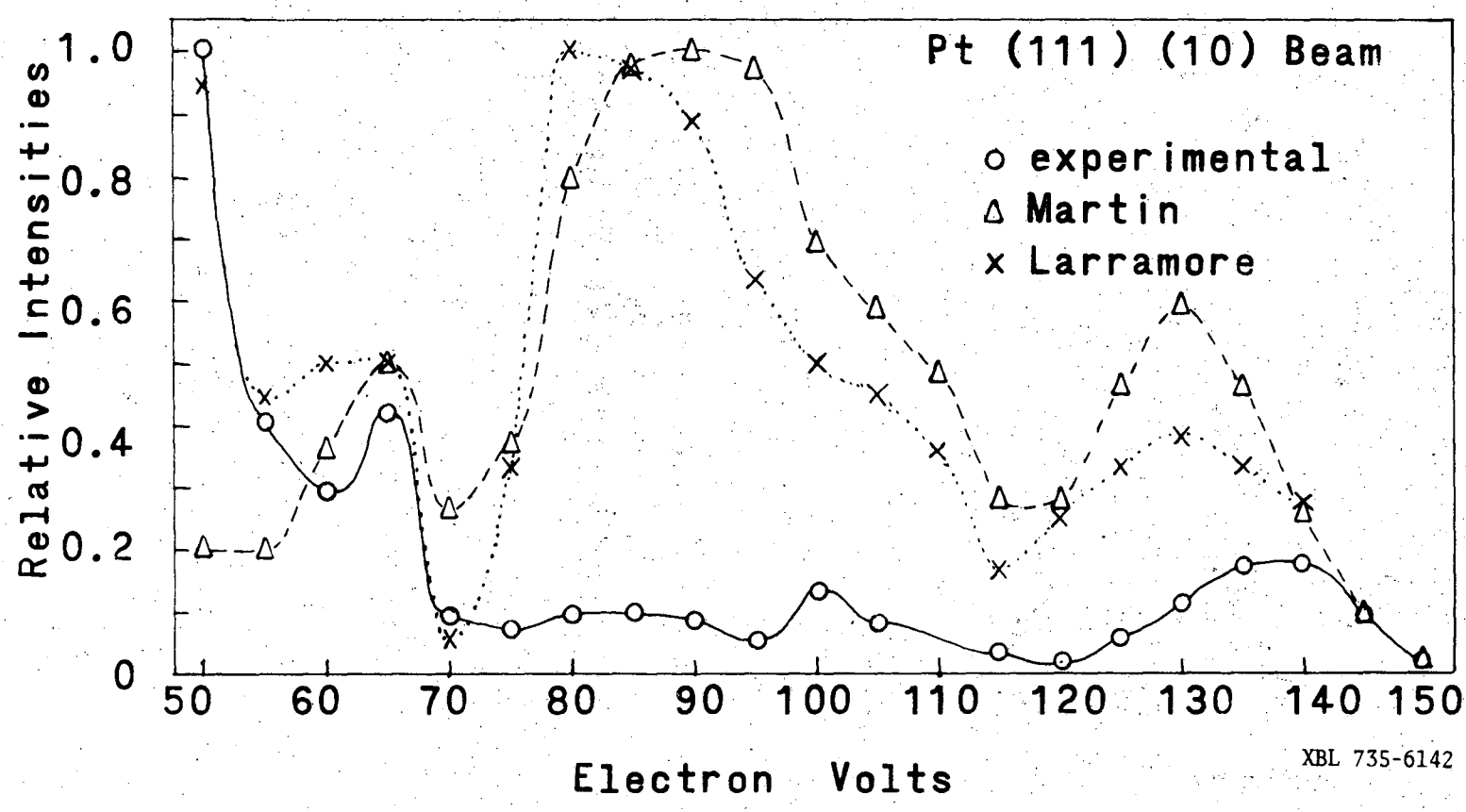

Fig. IV-2. I. vs V. curves for (10) beam of Pt(111) from experiment and multiple scattering theory, $\theta=\phi=0°$.

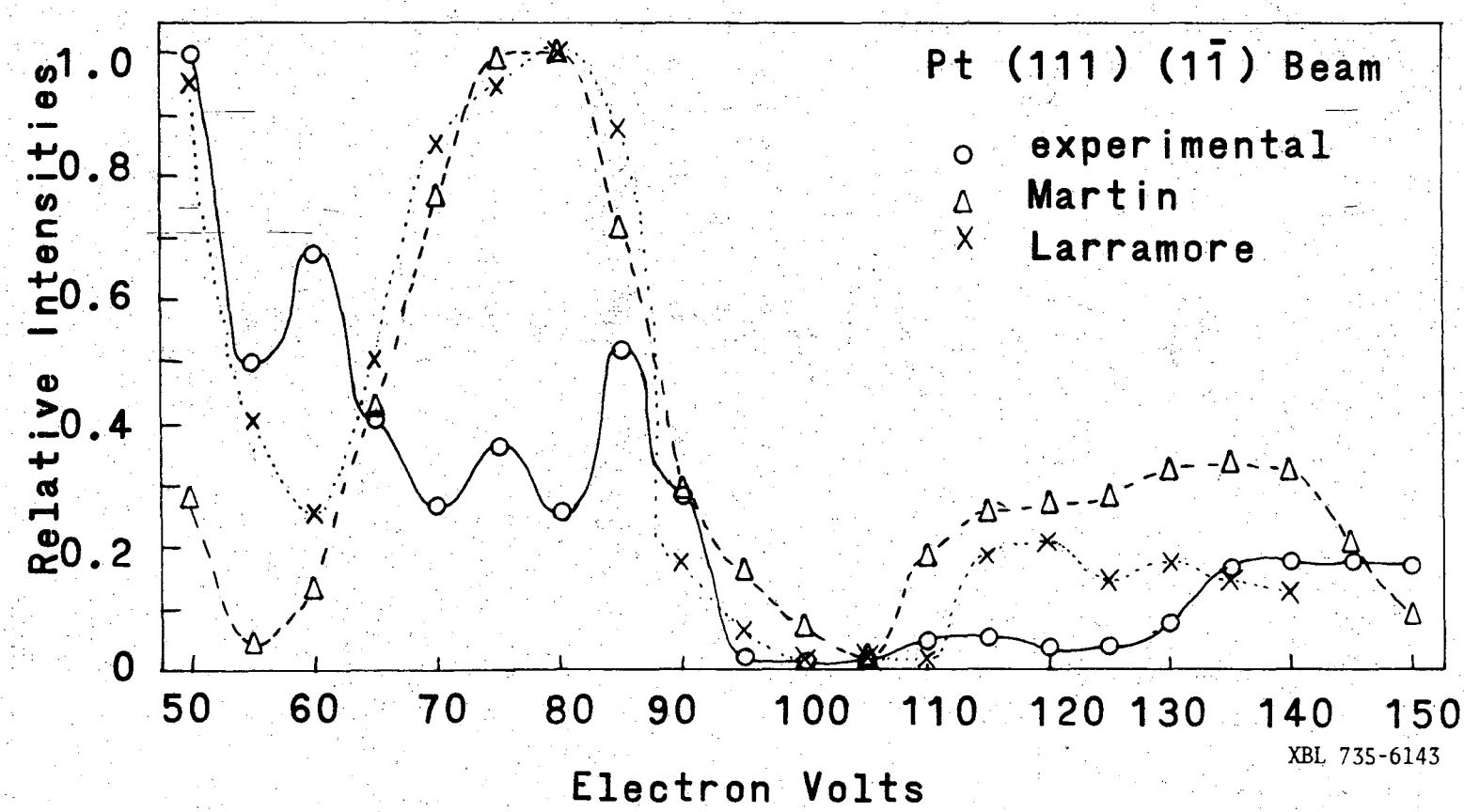

Fig. IV-3. I. vs V. curves for (1$\bar{1}$) beam of Pt(111) from experiment and multiple scattering theory, $\theta=\phi=0°$.

The intensities of some of the beams of the (5×1) structure characteristic of the clean surface of the (100) face of platinum have been previously measured by H. H. Farrell using a spot photometer.[29] The intensities were not normalized by the incident beam current and this would tend to increase the intensities at higher beam voltages. The value of ϕ is not reported and this also affects the measured intensities. Considering this, and also the fact that two different techniques were used and that intensities from this pattern are difficult to measure, the overall agreement is acceptable. Figures IV-4 to IV-8 plot relative intensities versus voltage for the five beams previously measured by the spot photometer technique and compare them with normalized relative intensities calculated from photographs. In each figure the two curves have been normalized to the value of the largest peak to facilitate comparison. Farrell measured the (00) beam at $\theta = 3°$ while the photographic data for this beam were taken at $\theta = 7°$. This may account for the fact that the intensity of the new curve falls off much more rapidly than Farrell's. Agreement for the fractional order beams is fairly good and both curves show their intensities decreasing with increasing voltage. This is expected since the fractional order beams are the result of the surface structure and at higher energies the contribution from the bulk structure would tend to increase. The only major disagreement occurs in the (11) beam where the peak at 135 volts in our results does not appear in the previous work and no explanation is currently available.

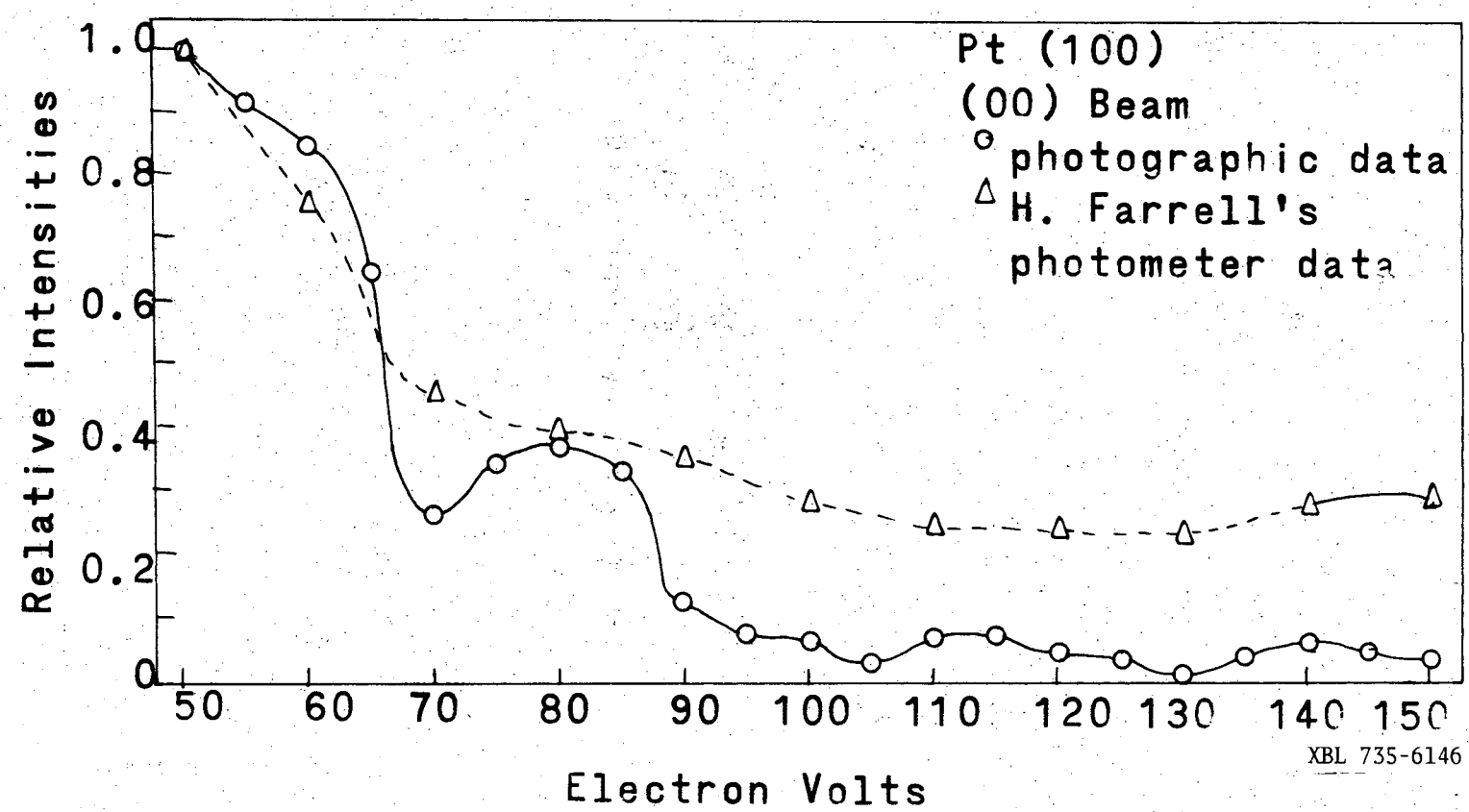

Fig. IV-4. Comparison of I. vs V. curves normalized to the largest peak, for (00) beam of (5×1), $\theta=7°$ and $\phi=2°$ photographic data, $\theta=3°$ in photometer data.

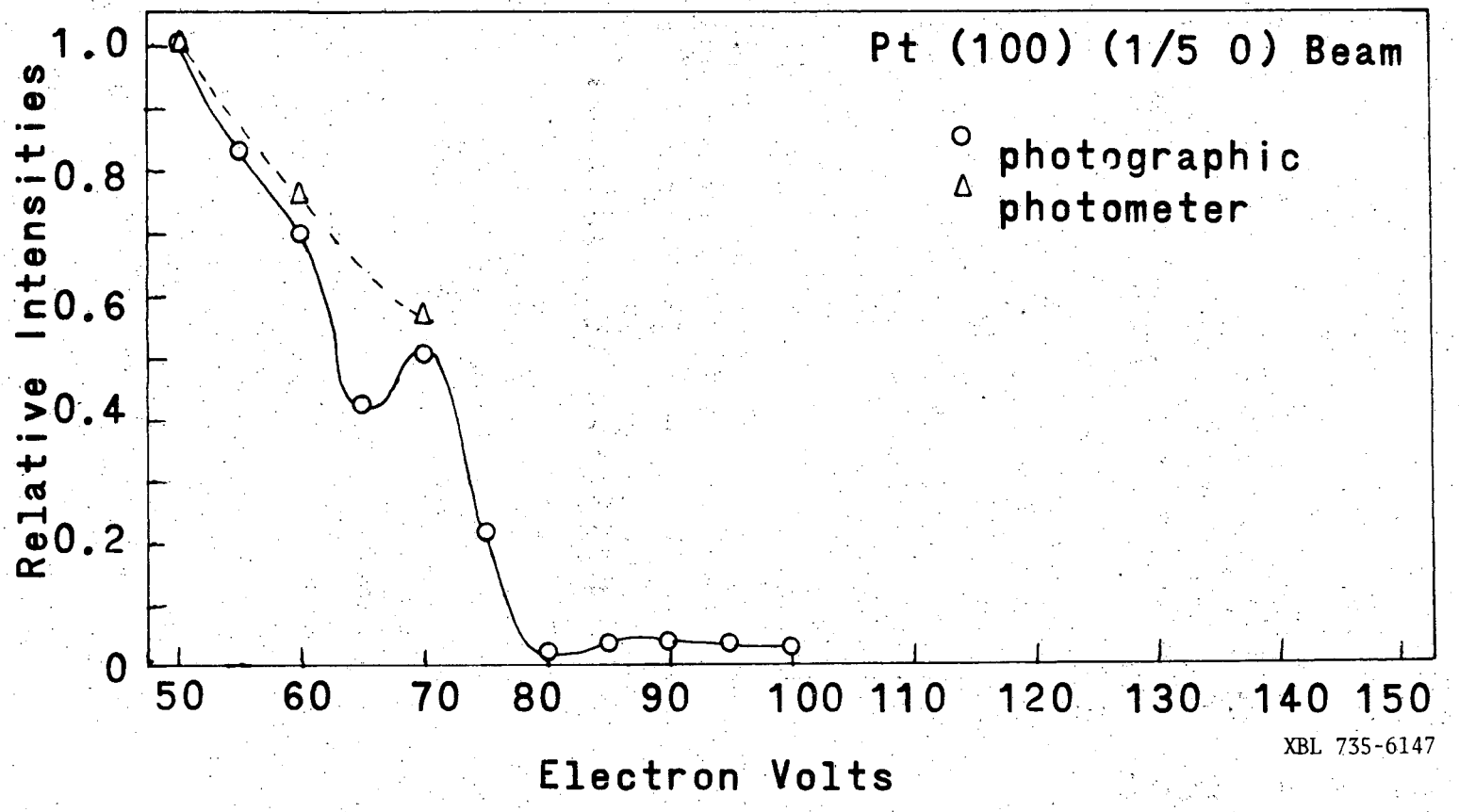

Fig. IV-5. Comparison of I. vs V. curves normalized to the largest peak for (1/5 0) beam of (5×1) $\theta=0°$ for both, $\phi=2°$ for photographic data.

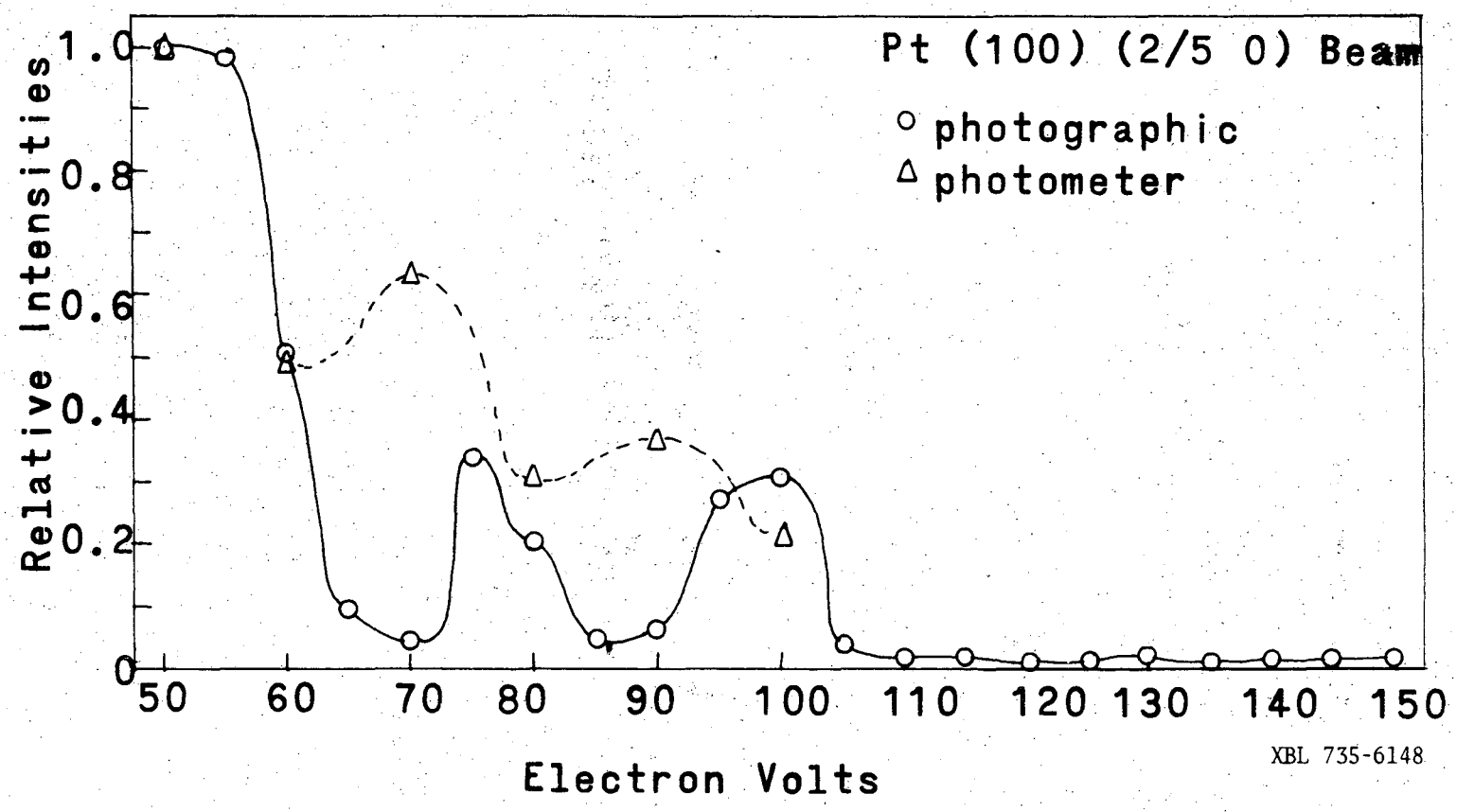

Fig. IV-6. Comparison of I. vs V. curves normalized to the largest peak for (2/5 0) beam of 5×1 $\theta=0°$ for both, $\phi=2°$ for photographic data.

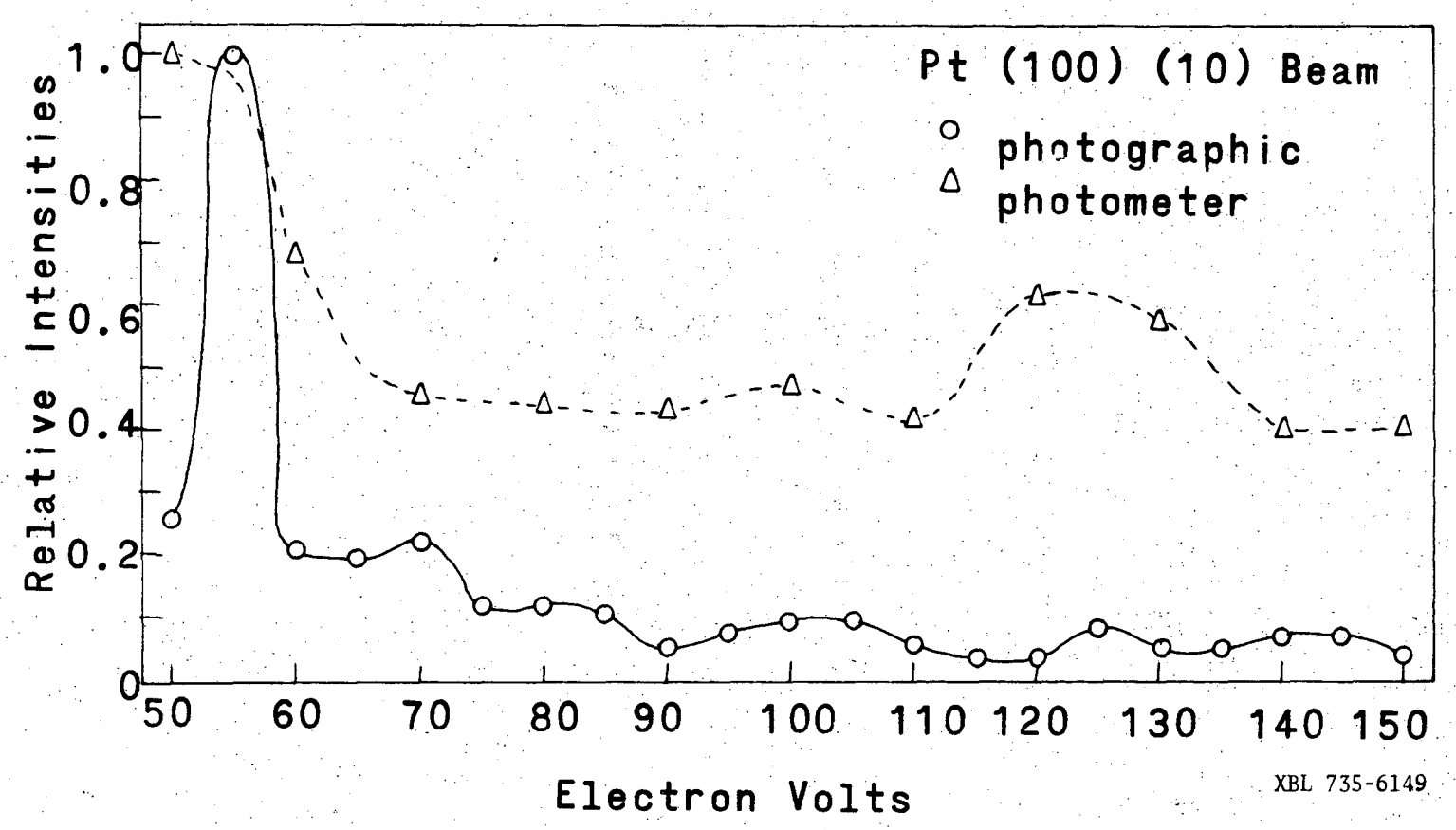

Fig. IV-7. Comparison of I. vs V. curves normalized to the largest peak for (10) beam of (5×1), $\theta=0°$ for both, $\phi=2°$ for photographic data.

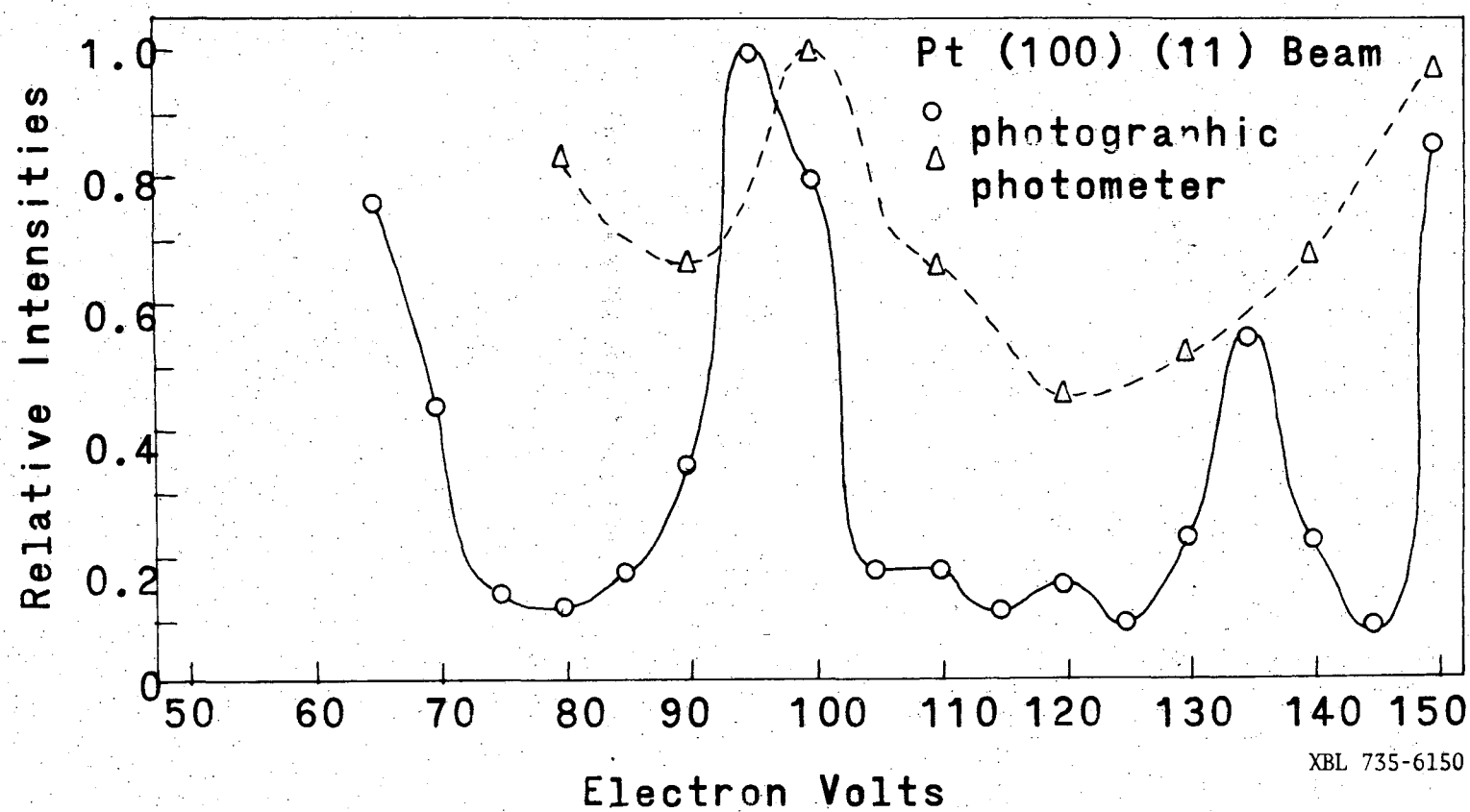

Fig. IV-8. Comparison of I. vs V. curves normalized to the largest peak for (11) beam of (5×1), θ=0° for both ϕ=2° for photographic data.

CONCLUSION

A method for obtaining normalized relative intensities from photographs of the diffraction pattern has been developed. Intensities measured in this way were compared with intensities measured by a spot photometer for the specular beam of Pt(111) and for several of the beams of the (5×1) surface structure of Pt(100) and agreed quite well. Using the photographic technique, intensities of the diffraction beams from the (111) and (100) faces of platinum and from the surface structure formed by the adsorption of propene on Pt(111) have been measured. The experimental results from Pt(111) were compared with intensities calculated by programs based on LEED dynamical scattering theory and show limited agreement. It appears that the electron self energy parameters used in these calculations must be adjusted to increase inelastic damping and sharpen the structure in the intensity curves. Perhaps a basic reevaluation of the pseudopotential used to calculate the phase shifts will also be necessary since it is not certain that all of the approximations used to calculate the ion core in the muffin-tin approximation are valid for a heavy scatterer like platinum. The recent development of averaging techniques to eliminate multiple scattering may make this a moot point if they prove successful for materials like platinum. However, that remains to be seen and so these experiments were performed in order to compare the results with those calculated using multiple scattering theory. It is hoped that the structure analysis of propene on platinum will be performed soon.

0 0 0 0 5 9 0 0 9 3 5

ACKNOWLEDGEMENTS

It is customary to begin by acknowledging the debt owed to one's research advisor but it is difficult to do it adequately without sounding trite. Professor Gabor A. Somorjai is an amazing man whose extraordinary energy, relentless drive, and tireless enthusiam cannot help but impress his students and inspire them. I will always be grateful for meeting the other members of my research group for they helped me many times in their varied roles of friends, colleagues, and teachers. Graduate school would have been a much poorer experience without the friendship, assistance and ideas of John Gland who "showed me the ropes" both in research and in backpacking. I would also like to thank Steve Bernasek and Cliff Megerle, friends with whom I often commiserated or rejoiced after mutal experiences in the classroom and the laboratory. Fredrick Szalkowski has probably forgotten how he explained LEED technique to me on my second day in the group or his introduction to Auger Spectroscopy but I haven't. Although I never did an experiment on stepped surfaces I would have missed much in group seminars without Don Blakeley's help. To Emery Kozak who helped me time and again in improving my apparatus and turned vague discriptions into finished work I can only say thank you. Julien Patenaude had to deal with my complete ignorance of a machine shop and the fact that I actually completed a number of projects is an indication of his skill and patience. Without the encouragement and support of my family I

probably would not have completed college and certainly would not have considered graduate school. Finally, I would like to thank the Technical Typing Group for deciphering my handwriting and transforming it into something readable.

This research has been supported by the U. S. Atomic Energy Commission.

REFERENCES

1. C. Davisson and L. H. Germer, Proc. Natl. Acad. 14, 619 (1928).
2. G. A. Somorjai and H. H. Farrell in Advances Chem. Phys. 20, A. Prigogine and S. A. Rice, eds. (John Wiley & Sons, New York, 1971).
3. G. E. Larramore and C. B. Duke, Phys. Rev. B 5, 267 (1972).
4. D. W. Jepsen, P. M. Marcus, and F. Jona, Phys. Rev. B 5, 3933 (1972).
5. S. Y. Tong and T. N. Rhodin, Phys. Rev. Lett. 26, 711 (1971).
6. M. R. Martin and G. A. Somorjai, LBL-1124 preprint (1972) and Phys. Rev. B 7, 3607 (1973).
7. J. B. Pendry, J. Phys. Chem. 4, 2501 and 2514 (1971).
8. G. A. Somorjai, Principles of Surface Chemistry (Prentice Hall Inc., Englewood Cliffs, N. J. 1972).
9. J. L. Beeby, J. Phys. Chem, Series 2, 1, 82 (1968).
10. J. L. Beeby, Proc. Roy. Soc. A 279, 82 (1964).
11. J. L. Beeby, Proc. Roy. Soc. A 302, 113 (1967).
12. J. B. Pendry, J. Phys. Chem, Series 2, 2, 1215 (1969).
13. C. B. Duke and C. W. Tucker, Surface Sci. 15, 231 (1969).
14. G. E. Larramore and C. B. Duke, Phys. Rev. B 2, 4783 (1970).
15. S. Y. Tong and T. N. Rhodin, Phys. Rev. Lett. 26, 711 (1971).
16. M. R. Martin, LBL report 1418 (1972).
17. B. O. Pines and P. Nozieres, The Theory of Quantum Liquids Vol. 1 (Benjamin, New York 1966).

18. J. B. Pendry, J. Phys. Chem., Series 2, 2, 2283 (1969).

19. D. W. Jepsen, L. M. Marcus and F. Jona, Phys. Rev. Lett. 26, 1365 (1971).

20. J. B. Pendry, J. Phys. Chem., Series 2, 2, 2273 (1969).

21. E. A. Wood, J. Appl. Phys. 35, 1306 (1964).

22. H. B. Lyon, Ph.D. thesis, University of California, Berkeley (1967).

23. R. W. Joyner, J. L. Gland, and G. A. Somorjai, LBL report 414 (1971).

24. Mees, The Theory of the Photographic Process (MacMillan & Co. New York 1942, revised 1952).

25. C. DeVere, Cathode-Ray Tubes (Tektronix, Inc. Beaverton, Oregon 1967).

26. F. Jona, IBM J. of Res. Develop. 14, 4 (1970).

27. M. R. Martin (private communication).

28. G. E. Larramore (private communication).

29. H. H. Farrell, Ph.D. thesis, University of California, Berkeley (1969).

LEGAL NOTICE

This report was prepared as an account of work sponsored by the United States Government. Neither the United States nor the United States Atomic Energy Commission, nor any of their employees, nor any of their contractors, subcontractors, or their employees, makes any warranty, express or implied, or assumes any legal liability or responsibility for the accuracy, completeness or usefulness of any information, apparatus, product or process disclosed, or represents that its use would not infringe privately owned rights.

TECHNICAL INFORMATION DIVISION
LAWRENCE BERKELEY LABORATORY
UNIVERSITY OF CALIFORNIA
BERKELEY, CALIFORNIA 94720